

# UNIFIED NEURAL SOLVERS FOR GENERAL TSP AND MULTIPLE COMBINATORIAL OPTIMIZATION TASKS VIA PROBLEM REDUCTION AND MATRIX ENCODING

**Anonymous authors**

Paper under double-blind review

## ABSTRACT

Various neural solvers have been devised for combinatorial optimization (CO), which are often tailored for specific problem types, ranging from TSP, CVRP to SAT, etc. Yet, it remains an open question how to achieve universality regarding problem representing and learning with a general framework. This paper first proposes **RedCO**, to unify a set of CO problems by reducing them into the *general* TSP form featured by distance matrices. The applicability of this strategy is dependent on the efficiency of the problem reduction and solution transition procedures, which we show that at least ATSP, HCP, and SAT are readily feasible. The hope is to allow for the effective and even simultaneous use of as many types of CO instances as possible to train a neural TSP solver, and optionally finetune it for specific problem types. In particular, unlike the prevalent TSP benchmarks based on Euclidean instances with 2-D coordinates, our focused domain of general TSP could involve non-metric, asymmetric or discrete distances without explicit node coordinates, which is much less explored in TSP literature while poses new intellectual challenges. Along this direction, we devise two neural TSP solvers with and without supervision to conquer such matrix-formulated input, respectively: 1) **MatPOENet** and 2) **MatDIFFNet**. The former is a reinforcement learning-based sequential model with pseudo one-hot embedding (POE) scheme; and the latter is a Diffusion-based generative model with the mix-noised reference mapping scheme. Extensive experiments on ATSP, 2DTSP, HCP- and SAT-distributed general TSPs demonstrate the strong ability of our approaches towards arbitrary matrix-encoded TSP with structure and size variation. Source code and data will be made public.

## 1 INTRODUCTION

Beyond heuristics, learning-based neural solvers have shown success in solving combinatorial optimization (CO) problems<sup>1</sup>. While designing neural solvers for a specific type e.g., TSP has been a popular pursuit (Khalil et al., 2017; Vinyals et al., 2015), yet such a problem type-specific paradigm can be restrictive in real-world with immense problem diversity, which prompts the following question:

- Can we develop a **general framework** capable of learning a range of CO problems on graph in a unified manner?

In this paper, we resort to utilizing **problem reduction**, namely transformation between different problem types which is in fact largely neglected by previous research. By the theory of computational complexity, any NP problem can be transformed (or in a more professional terminology, reduced) into an NP-Complete (NPC) problem in polynomial time, and every NP problem can be reduced to an NP-hard problem in polynomial time (Lewis, 1983; Van Leeuwen, 1991). The famous Karp’s 21 NPC problems (Karp, 1972) exemplify the polynomial-time reduction between 21 NPC CO problems.

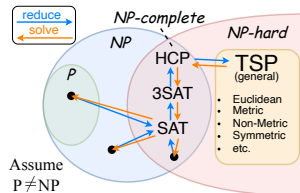


Figure 1: CO problems and the polynomial-time reduction. HCP, 3SAT and SAT are used as case studies in this paper.

<sup>1</sup>Methods discussed or proposed in this paper, are anchored to CO problems on graphs, especially those technically reducible or structurally similar to general TSP, i.e., feasibly characterizable via matrix formulation.

Table 1: Comparison of different current works with the key word “multi-task solver”. Refer to Table 6 in Appendix B.4 for a more thorough comparison of recent related works.

Method	MTCO (Li & Liu, 2023)	ASP (Wang et al., 2024)	MAB-MTL (Wang & Yu, 2023)	MVMoE (Zhou et al., 2024)	RedCO (Ours)	
Evaluated Problems	PFSP	2DTSP, CVRP	TSP, CVRP, OP, KP	VRPs	ATSP, 2DTSP, DHCP, 3SAT	
Applicable Problems		N/A (no solver is proposed)	✓	Limited to VRP variants	{problem $\mathcal{P}   \mathcal{P} \leq_P \text{general TSP}$ }	
Multi-Task					✗	✓
Multi-Scale					✓	✓
Single Solver	✗	✗	✓	✓		
Solver Type	Quadratic Programming	Evaluated on ML-based ones	ML-based	ML-based	ML-based	
Brief Description	Enhance PFSP solving via knowledge transferring between similar instances	A model-/problem-agnostic training framework to improve generalizability	A multi-task neural solver for specific problems via multi-armed bandits	A multi-variant VRP solver with hierarchical gating mechanism	A neural CO framework with two solvers for problems reducible to general TSP	

Specifically, by introducing the general Traveling Salesman Problem (general TSP, see Def. 1) as the reduction endpoint, one can construct a problem reduction tree as shown in Fig. 1, suggesting the potential of training a general TSP solver to tackle problems within the reduction tree. While theoretically, other NP-hard problems, e.g., mixed integer linear programming (MILP) could also serve as the reduction endpoint (Zhang et al., 2023), TSP has already fostered extensive research attention in neural solvers in recent literature (U et al., 2021). In fact, existing machine learning research on (end-to-end) MILP neural networks are still very limited (Zhang et al., 2023), compared with the emerging progress in TSP (Li et al., 2023; Ye et al., 2024b; Drakulic et al., 2023).

In the context of developing a general neural TSP solver for various CO problems as discussed above, the reduced TSP instances in fact can be represented by an arbitrary distance matrix in both its size as well as its elementary value, far beyond the popular 2D points form (Kwon et al., 2020) in the well-studied Euclidean space. In another word, it can be no longer a metric space and the distance may break the triangular inequality. Currently, Transformer (Vaswani et al., 2017) and graph neural network (GNN) have become popular backbones for neural TSP solvers (Joshi et al., 2019; Kool et al., 2018) where the 2D coordinates of the points are often used as node features, which largely hinges the research scope of the TSP world. For the general TSP with arbitrary matrix as input, it is technically nontrivial to achieve effective featuring of the problem instances with only pair-wise relationships and have non-deterministic node numbers (Joshi et al., 2020). To address such challenges, this paper proposes a novel framework called RedCO and two corresponding neural solvers (MatPOENet and MatDIFFNet) that innovatively improves prevalent Transformer and Diffusion models as matrix encoder for general TSP learning and solving. **Our contributions can be summarised as follows:**

- We conceptualize **RedCO**, namely Reductive Combinatorial Optimization learning framework, leveraging the rich expressivity of general TSP with arbitrary positive-valued matrix for unified representation of multiple CO problems (where reducible). We also construct standard datasets benchmarking the under-explored capacity of the general TSP world accordingly. This practice, to our best knowledge, has not been performed, especially in the context of machine learning for CO.
- We propose **MatPOENet**, namely Matrix encoding Network with Pseudo One-hot Embedding, a reinforced Transformer-based model which utilizes a novel size-agnostic node embedding to aid instance input, thereby significantly improving model scalability and performance of general TSP.
- We propose **MatDIFFNet**, namely Matrix encoding Diffusion Network, a supervised diffusion-based model which leverages a novel mix-noised reference map module, thus extending the promising ability of generative model for Euclidean TSP solving to matrix-formulated general TSP.
- We instantiate RedCO with the above two proposed neural backbones and one more existing method, DIMES, and conduct experiments on general TSP with four types of CO problem distributions, i.e., ATSP, 2DTSP, DHCP, and 3SAT. Experiments show that measuring either the average TSP tour length or the average rate that solvers find optimal solutions for decisive tasks, our best-performing methods beat compared neural approaches, and outperform the strong heuristic LKH in some cases.

## 2 RELATED WORKS

**Multi-Task CO Solvers.** To our knowledge, this is the first work that combines neural matrix encoding general TSP solver and unified multi-task CO learning. While similar concepts, e.g., “multi-task solver”, “universal solver”, etc., have also appeared in recent literature, they often denote quite different approaches and functionalities. For example, **MTCO** (Li & Liu, 2023) devises a “multi-task” CO framework which measures the similarity between CO problems, and then transfers knowledge between similar instances within the same problem type to gain search speed-ups in its quadratic programming solver. However, it solely focuses on the permutation flowshop scheduling problem (PFSP) and is not specifically designed for learning-based neural solvers, making the term “multi-task”

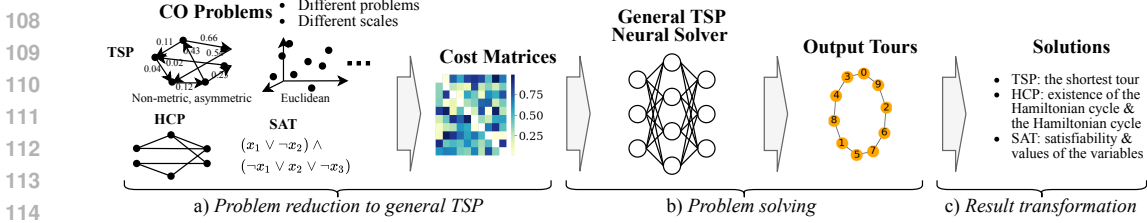


Figure 2: The 3-step workflow of the reductive CO (RedCO) learning framework.

in its title misleading from a learning perspective and irrelevant to the theme of this paper. **ASP** (Wang et al., 2024) proposes a “universal” framework to address generalization issues of neural CO solvers, which iteratively improves the generalizability to different distributions (including scales). ASP proposes a model-/problem-agnostic training policy to improve generalizability. However, no specific new solver is proposed, which we believe is technically nontrivial to deal with different problems. In **MAB-MTL** (Wang & Yu, 2023), authors propose a multi-armed bandit framework to train a neural solver with a shared encoder but different header and decoder. Yet, as the header and decoder necessitate customized designs for specific problems, the solver cannot be readily applied to unseen problems, restricting its applicability to the training dataset comprising four tasks. **MVMoE** (Zhou et al., 2024) proposes a “multi-task” vehicle routing solver with mixture-of-experts and a hierarchical gating mechanism to enhance the model capacity with good computational complexity. However, its applicable problems are also limited to variants of VRPs. Table 1 outlines the disparities between representative existing works and ours, highlighting the uniqueness and novelty of our work. More recent works like **MTNCO** (Liu et al., 2024), **UNCO** (Jiang et al., 2024), and **GOAL** (Drakulic et al., 2024), etc., are discussed in Appendix B.4.

**General TSP Solvers.** Besides traditional solvers and heuristics, neural methods for TSP with coordinates have been well studied in literature (Kool et al., 2018; Kwon et al., 2020; Li et al., 2023; Qiu et al., 2022; Sun & Yang, 2023; Vinyals et al., 2015; Xin et al., 2021). However, neural solvers for general TSP are much more challenging due to a lack of effective and scalable neural networks to handle the pairwise distance information. To our best knowledge, few works have demonstrated comparable capability of general TSP solving without major revisions to the model architecture or learning paradigm. **MatNet** (Kwon et al., 2021) proposes a Transformer-based solver for asymmetric TSP (ATSP) which first takes distance matrices as input. However, the adopted one-hot embedding has limitations in dealing with arbitrarily large matrix and its implementation typically includes a preset value of maximum size, restricting its ability to generalize to arbitrarily large scales. **GLOP** (Ye et al., 2024b) proposes a neural partition and conquering framework that can incorporate matrix encoding models like MatNet as local reviser for general TSP solving, thus its performance is largely relied on the adopted local solver. **BQ-NCO** (Drakulic et al., 2023) proposes leveraging bisimulation quotienting to enhance out-of-distribution robustness on CO problems, which is capable of solving ATSP via Markov Decision Process (MDP) formulation. **DIMES** (Qiu et al., 2022) utilizes a GNN to encode both node features (coordinates) and edge features (distances) and is trained by model-agnostic meta-learning and deep reinforcement learning. It can be adapted for general TSP solving with minor modifications to the node features, at the cost of subpar results.

Additional related works are introduced in detail in Appendix B, including exact solvers, heuristic solvers for general TSP, autoregressive, non-autoregressive neural solvers and neural-heuristic solvers for 2DTSP, divide-and-conquer methods for large routing problems, as well as specific solvers for other covered CO problems (HCP, SAT, etc.).

### 3 PRELIMINARIES

#### 3.1 COVERED CO PROBLEMS

**Definition 1** (Traveling Salesman Problem (TSP)). *Given a complete, directed or undirected graph without self-loops denoted by  $G = (\mathcal{V}, \mathcal{E})$  ( $\mathcal{V} = \{1, 2, \dots, N\}$ : the node set,  $\mathcal{E}$ : the edge set) along with a cost matrix  $\mathbf{C}$  of the shape  $N \times N$  where the entry  $\mathbf{C}_{ij}$  is the cost for edge  $(i, j) \in \mathcal{E}$ , the problem is to find the tour  $\tau = (i_1, \dots, i_N)$  to minimize the cost  $\sum_{k=1}^{N-1} \mathbf{C}_{i_k i_{k+1}} + \mathbf{C}_{i_N i_1}$ .*

**Definition 2** (Hamiltonian Cycle Problem (HCP)). *Given a directed or undirected graph  $G = (\mathcal{V}, \mathcal{E})$ , the problem is to determine whether there exists a Hamiltonian cycle in  $G$ .*

**Algorithm 1** The training pipeline of RedCO.

---

**Input:** Problems  $\{\mathcal{P}\}$  reduced to general TSP, batch size  $B$ , a general TSP solver  $\mathcal{S}$  handling instances of different scales.

**repeat**

Select a problem from  $\{\mathcal{P}\}$  and generate a batch of  $B$  instances of the problem at the same scale;

Reduce the instances to general TSP instances with cost matrices  $\{\mathbf{C}^{(b)}\}_{b=1}^B$ ;

Train  $\mathcal{S}$  with the input instances  $\{\mathbf{C}^{(b)}\}_{b=1}^B$ ;

**until** the training of  $\mathcal{S}$  converges;

---

**Definition 3 (Boolean Satisfiability Problem (SAT) in conjunctive normal form (CNF)).** SAT aims to determine the existence of an interpretation that satisfies a given Boolean formula. A Boolean formula in CNF is represented by a conjunction (denoted by  $\wedge$ ) of clauses that are disjunctions (denoted by  $\vee$ ) of variables. For example,  $(x_1 \vee \neg x_2) \wedge (\neg x_1 \vee x_2 \vee \neg x_3)$  is a SAT instance of two clauses  $(x_1 \vee \neg x_2)$  and  $(\neg x_1 \vee x_2 \vee \neg x_3)$ , and three variables  $x_1, x_2$  and  $x_3$ .

Special cases of TSP are defined according to the properties of the cost matrix  $\mathbf{C}$ :

- *Metric.* A TSP is metric if the triangle inequality, i.e.,  $\mathbf{C}_{ij} + \mathbf{C}_{jk} \geq \mathbf{C}_{ik}$ , holds for any different three nodes  $i, j$ , and  $k$ . Specially, when  $\mathbf{C}$  is derived from coordinates in Euclidean space, the TSP is *Euclidean*.
- *Symmetric.* A TSP is symmetric if  $\mathbf{C}_{ij} = \mathbf{C}_{ji}$  for all  $i$  and  $j$ ; otherwise, it is *asymmetric*.

We use the term “*general TSP*” to refer to TSPs either metric or non-metric, symmetric or asymmetric. For HCP, without losing generality, we mainly discuss directed HCP (DHCP) in this paper. For SAT, a special case of SAT in CNF with at most 3 variables is named as 3-Satisfiability Problem (3SAT). Note any SAT problem can be reduced to 3SAT in polynomial time (Fouh et al., 2014). Throughout this paper, for consistent representation and unified evaluation, when we mention any problem type  $X$ , we prescribe a limit to its reduced general TSP formulation, i.e., differently distributed distance matrices only. Furthermore, note that a wider range of problems (e.g., VC, Clique, certain VRPs, FFSP, MIS, etc., as detailed in Appendix E.2), can be dealt with by our proposed methods.

### 3.2 POLYNOMIAL-TIME REDUCTION OF CO TO GENERAL TSP

The reduction relations of the covered CO problems in this paper can be summarized as  $3SAT \leq_P HCP \leq_P TSP$  ( $A \leq_P B$  means that the problem  $A$  can be reduced to  $B$  in polynomial time). The solutions can also be transformed from a TSP tour to the solution of the raw problem. The detailed illustration of instance reduction and proofs are provided in Appendix A.

## 4 METHODOLOGY

### 4.1 REDCO: REDUCTIVE CO LEARNING FRAMEWORK

As illustrated in Fig. 2, given a CO instance, RedCO works in a 3-step pipeline: a) reduce the instance to a general TSP instance with a distance matrix obtained by techniques in Sec. 3.2, b) feed the distance matrix to a trained general tsp solver and output a tour, and c) transform the output tour into the solution of the origin problem (efficiently). To prepare the training data, we build a problem pool with CO problems of different scales that can be reduced to general TSP (see Sec. 5.1 for details). During training, we randomly fetch problems from the pool, transform them to general TSP, and treat the general CO solver training as an equivalent task to train the general TSP solver. A concise pipeline is given in Algorithm 1. In the main context, we propose increments to two promising architectures in solving general TSP across scales: the Transformer-based MatPOENet, and the Diffusion-based MatDIFFNet, trained in the reinforcement (Williams, 1992) and supervised manner, respectively. We describe the two architectures in Sec. 4.2 and Sec. 4.3. To demonstrate the general applicability of RedCO to different backbone solvers, we additionally incorporate DIMES (Qiu et al., 2022), a neural model based on GNN and meta-reinforcement learning, into our RedCO framework. Details of model, training, and results of RedCO-DIMES are presented in Appendix E.1.

### 4.2 TRANSFORMER-BASED SOLVER: MATPOENET

**Overview.** As is known, MatNet (Kwon et al., 2021) is the first neural solver designed for matrix encoding and asymmetric TSP. To overcome the inherent drawback that vanilla MatNet cannot scale to arbitrary size of input due to its fixed initial node embeddings, we propose **MatPOENet**, namely

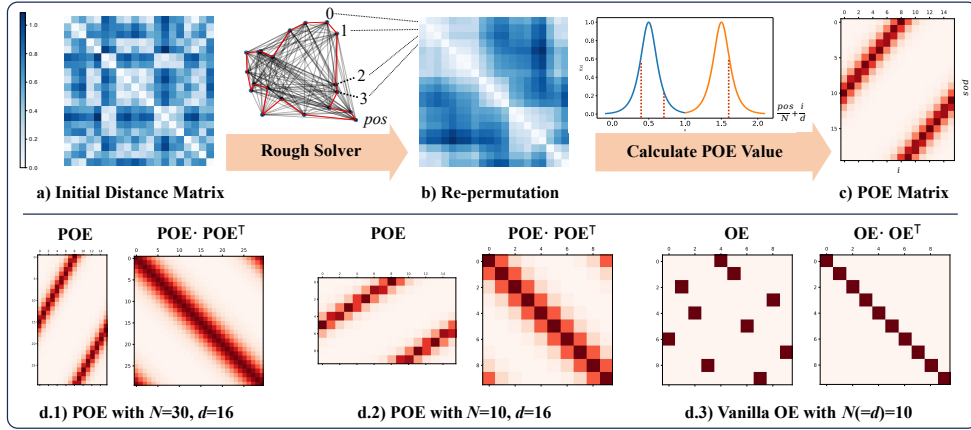


Figure 3: a-c) The three steps to generate the pseudo one-hot embedding (POE). d) The visualization of POE when  $N > d$  (d.1) and  $N < d$  (d.2) and one-hot embeddings (OE) (d.3), lighter blocks represent higher values. As the approximation of OE, POEs in Fig. d.1) and d.2) both achieve concentrating POE pairs of high dot products near the diagonal of the dot product matrix.

Matrix encoding Network with Pseudo One-hot Embedding for general TSP, which greatly improves model scalability as well as performance. MatPOENet utilizes an encoder-decoder Transformer architecture to learn features of each city in the TSP, and is trained with deep reinforcement learning scheme (DRL). Generally, the model takes two sets of initial node embeddings  $\mathbf{a}_0, \mathbf{b}_0$  and a distance matrix  $\mathbf{C}$  as input, and sequentially calculates the probability of nodes selected for the next position in the TSP tour via standard attention operations and a mask indicating whether a node has been visited. The model is trained using POMO (Kwon et al., 2020) by DRL. For each instance with distance  $\mathbf{C}$ ,  $N$  tours  $\{\tau^1, \dots, \tau^N\}$  with different starting nodes are sampled to calculate the policy gradient:

$$\nabla_{\theta} J(\theta) \approx \frac{1}{N} \sum_{n=1}^N (L(\tau^n) - b(\mathbf{C})) \nabla_{\theta} \log p_{\theta}(\tau^n | \mathbf{C}), \quad (1)$$

where  $L(\tau)$  is the length of tour  $\tau$ ,  $b(\mathbf{C}) = 1/N \sum_{n=1}^N L(\tau^n)$  is a baseline method, set as the mean tour length of the  $N$  tours. Mathematical details of the model and training process is deferred to Appendix C.1 and the general network structure is correspondingly illustrated in Fig. 4. The POE technique introduced in Sec 4.2.1 is the highlight of our design, taking its effect by assigning  $\mathbf{b}_0$  a non-trivial position embedding to largely elevate the performance and scalability of the model.

#### 4.2.1 PSEUDO ONE-HOT EMBEDDING

In vanilla MatNet, zero embedding and one-hot embedding is adopted for initial node embedding. However, the one-hot component is of fixed size and cannot accommodate arbitrary input matrix sizes. Thus, we seek an input size-agnostic encoder with dimension  $d$ , thereby dismissing the need for the one-hot embedding. As a solution, we propose the Pseudo One-hot Embedding (POE) in the continuous vector space to replicate the functionality of the vanilla one-hot embedding. We denote the input embedding as  $\mathbf{x}_i \in \mathbb{R}^d$  where  $i$  is the node index. When we are applying the model on large instances, i.e.,  $N > d$ , we can never ensure  $\mathbf{x}_i \cdot \mathbf{x}_j = 0, \forall i \neq j$  as with the one-hot embedding. That means, there will unavoidably be some bias on the similarities between embeddings. So naturally, we incorporate this bias into the POE design by assigning similar embeddings to nodes that are likely to be connected in the solution.

Specifically, the POE works by the following steps: **1) (Fig. 3 a)** We transform the input cost matrix into a tour, forming a closed loop by a rough solver. To ensure efficiency, we adopt the *nearest neighbor* (NN) heuristic as the rough solver, which can also be replaced by other possible choices. Subsequently, each node on the tour is assigned a position index denoted by  $pos$  ranging from 0 to  $N - 1$ . **2) (Fig. 3 b)**: We define an even function  $f: [-\frac{1}{2}, \frac{1}{2}] \rightarrow (0, 1)$  with an ‘‘impulse-like’’ shape, as depicted in Fig. 3 b). The POE is then generated based on  $f$ , with empirical success found using  $f(x) = 1/\cosh(100x)$ . **3) (Fig. 3 c)**. We rotationally shift  $f$  along the tour for different positions, and generate POEs by sampling values from  $f$ . Mathematically, the  $i$ -th entry of the POE for position

270  $pos$  can be given by:

$$271 \mathbf{P}_{pos,i} = \begin{cases} 272 f\left(\frac{pos}{N} + \frac{i}{d} - \frac{1}{2}\right) & \text{if } \frac{pos}{N} + \frac{i}{d} \leq 1 \\ 273 f\left(\frac{pos}{N} + \frac{i}{d} - \frac{3}{2}\right) & \text{if } \frac{pos}{N} + \frac{i}{d} > 1 \end{cases}. \quad (2)$$

275 The POE matrix  $\mathbf{P}$  then becomes the substitution of  $\mathbf{B}^0$  in the vanilla MatNet. To visualize the  
276 similarity between POE and the original one-hot embeddings, Fig. 3 d.1-3) shows different cases of  
277 the POE and one-hot embeddings.

### 279 4.3 DIFFUSION-BASED SOLVER: MATDIFFNET

280 **Overview.** Generative methods gain considerable attention and show promising performance in  
281 TSP solving. Prominent models for the generative objective encompass diffusion models (e.g., DI-  
282 FUSCO (Sun & Yang, 2023) and T2T (Li et al., 2023)) and variational autoencoders (VAE) (Hottung  
283 et al., 2021a). These representative works demonstrate good feasibility and competitive results of dif-  
284 fusion model solving TSP in the Euclidean space. However, a robust generative backbone for *general*  
285 *matrix-formulated* (A)TSP which finely adapts our RedCO framework has yet to be proposed. To fill  
286 this gap, we devise **MatDiffNet**, namely Matrix encoding Diffusion Network for general TSP, which  
287 can also be seamlessly incorporated in our RedCO pipeline for multi-task and multi-scale unified  
288 training and solving. MatDiffNet is inspired by and developed upon Sun & Yang (2023) and Li et al.  
289 (2023), endeavoring to characterize a distribution of high-quality solutions for a given instance, i.e.,  
290 estimating  $p(\mathbf{S}|\mathbf{C})$ , where  $\mathbf{S}$  is the solution distribution and  $\mathbf{C}$  the distribution of distance matrix. the  
291 general framework of diffusion includes a forward noising and a reverse denoising Markov process.  
292 The noising process takes the initial solution  $\mathbf{S}_0$  and progressively introduces noise to generate a  
293 sequence of latent variables  $\mathbf{S}_{1:T}$ . The denoising process is learned by the model, which starts from  
294 the final latent variable  $\mathbf{S}_T$  and denoises  $\mathbf{S}_t$  at each time step to generate the preceding variables  
295  $\mathbf{S}_{t-1}$  based on the instance  $\mathbf{C}$ , eventually recovering the target data distribution. The formulation  
296 of the denoising process is expressed as  $p_\theta(\mathbf{S}_{0:T}|\mathbf{C}) = p(\mathbf{S}_T) \prod_{t=1}^T p_\theta(\mathbf{S}_{t-1}|\mathbf{S}_t, \mathbf{C})$ . The training  
297 optimization aims to align  $p_\theta(\mathbf{S}_0|\mathbf{C})$  with the data distribution  $q(\mathbf{S}_0|\mathbf{C})$  using ELBO:

$$298 \mathcal{L} = \mathbb{E}_q \left[ \sum_{t>1} D_{KL} [q(\mathbf{S}_{t-1}|\mathbf{S}_t, \mathbf{S}_0) \parallel p_\theta(\mathbf{S}_{t-1}|\mathbf{S}_t, \mathbf{C})] - \log p_\theta(\mathbf{S}_0|\mathbf{S}_1, \mathbf{C}) \right] + C. \quad (3)$$

301 We defer the mathematical elaboration of discrete diffusion process (derivation through Bayesian  
302 theorem, transition probability matrix, etc.) to Appendix C.2 and the general network structure is  
303 correspondingly illustrated in Fig. 5. The adaptive scheme proposed to enable matrix-input for our  
304 generative general TSP solver is detailed in the following Sec. 4.3.1.

#### 306 4.3.1 MIX-NOISED REFERENCE MAP AND DUAL FEATURE CONVOLUTION

307 In previous works, graph-based diffusion networks for TSP takes two core inputs for the GNN encoder.  
308 One is the Euclidean 2D coordinates as initial node features, and the other is the noised reference  
309 map which forms the initial edge embedding. However, in general TSP formulation, no coordinates  
310 is available while an arbitrary distance matrix is instead provided. We endeavor to maintain the best  
311 compatibility with previous design principles, thus proposing to combine the distance matrix and the  
312 noised label matrix to obtain a mix-noised reference map to replace the original  $\mathbf{x}_t$  to leverage edge  
313 information from pair-wise distances and enrich the initial edge embedding. Additionally considering  
314 the asymmetry of the distance matrix for general TSP and inspired by the scheme adopted in Kwon  
315 et al. (2021), we introduce two random vectors as pseudo coordinates for both "from" points and "to"  
316 points as node inputs, which will be updated respectively in subsequent GNN aggregations.

317 **Mix-Noised Reference Map.** The fusion of distance matrix  $\mathbf{C} \in \mathbb{R}^{N \times N}$  and original noised  
318 reference map  $\mathbf{x}_t \in \mathbb{R}^{N \times N}$  is learned by a multilayer perceptron (MLP) with two input nodes and a  
319 single output node and biases, conforming to that of vanilla MatNet. Mathematically, the mix-noised  
320 reference map  $\mathbf{x}_t^C \in \mathbb{R}^{N \times N}$  for the diffusion encoder can be calculated as follows. First, stack  $\mathbf{C}$  and  
321  $\mathbf{x}_t$  along the last dimension to gain a mixture tensor  $M \in \mathbb{R}^{N \times N \times 2}$ , where  $N$  denotes the number of  
322 nodes and the batch size is omitted. Then, linear and activating operations are performed on  $M$ :

$$323 \mathbf{x}_t^C = W_{\text{mix}2} (\text{ReLU} (W_{\text{mix}1}(M))). \quad (4)$$

Subsequently,  $\mathbf{x}_t^C$  is used to compute the initial edge embedding for the GNN via sinusoidal featurizing of each input element respectively:

$$\tilde{e}_i = \text{concat} \left( \sin \frac{e_i}{T^{\frac{d}{4}}}, \cos \frac{e_i}{T^{\frac{d}{4}}}, \sin \frac{e_i}{T^{\frac{d}{4}}}, \cos \frac{e_i}{T^{\frac{d}{4}}}, \dots, \sin \frac{e_i}{T^{\frac{d}{4}}}, \cos \frac{e_i}{T^{\frac{d}{4}}} \right), \quad (5)$$

where  $e_i$  denotes the  $i$ -th value of the  $N^2$  entries in  $\mathbf{x}_t^C$ ,  $d$  is the embedding dimension,  $T$  is a large number (usually selected as 10000),  $\text{concat}(\cdot)$  denotes concatenation.

**Dual Feature Convolution.** Let  $t^0 \in \mathbb{R}^{d_t}$ , where  $d_t$  is the time feature embedding dimension.  $e$  is the mix-noised reference map calculated above. As for node features, deviating from the widely used GCN model (Joshi et al., 2019) that learns single node representation, we introduce  $x_A, x_B \in \mathbb{R}^{N \times 2}$ , two random generated pseudo coordinates as initial node embeddings for the asymmetric nodes in general TSP, and maintain two distinct node features with two sets of learnable parameters throughout the cross-layer convolution operations:

$$x_{A,i}^{l+1} = x_{A,i}^l + \text{ReLU}(\text{BN}(W_{A,1}^l x_{A,i}^l + \sum_{j \sim i} G_{ij}^l \odot (W_{A,2}^l x_{A,j}^l + W_{B,2}^l x_{B,j}^l))), \quad (6)$$

$$x_{B,i}^{l+1} = x_{B,i}^l + \text{ReLU}(\text{BN}(W_{B,1}^l x_{B,i}^l + \sum_{j \sim i} G_{ij}^l \odot (W_{A,2}^l x_{A,j}^l + W_{B,2}^l x_{B,j}^l)^\top)), \quad (7)$$

$$e_{ij}^{l+1} = e_{ij}^l + \text{ReLU}(\text{BN}(W_3^l e_{ij}^l + W_{A,4}^l x_{A,i}^l + W_{B,4}^l x_{B,j}^l)) + W_5^l(\text{ReLU}(t^0)), \quad (8)$$

$$G_{A,ij}^l = \frac{\sigma(e_{ij}^l)}{\sum_{j' \sim i} \sigma(e_{ij'}^l) + \epsilon}, \quad G_{B,ij}^l = \frac{\sigma((e_{ij}^l)^\top)}{\sum_{j' \sim i} \sigma((e_{ij'}^l)^\top) + \epsilon}, \quad (9)$$

where  $W_{A,1}, W_{B,1}, \dots, W_5 \in \mathbb{R}^{h \times h}$  denote the model weights,  $G_{ij}^l$  denotes the dense attention map for element-wise gating. The convolution operation integrates the edge feature to accommodate the significance of edges in routing problems. The final prediction of the edge heatmap in TSP is  $\mathbf{H}_{i,j} = \text{Softmax}(\text{norm}(\text{ReLU}(W_e e_{i,j}^l)))$  for subsequent decoding and searching process.

## 5 EXPERIMENTS

### 5.1 EXPERIMENTAL SETUP

**Hardware.** MatPOENet is trained on an NVIDIA RTX3090 24GB GPU with AMD 3970X 32-Core CPU for  $N \leq 50$ , and on an RTX8000 48GB GPU with Intel Xeon W-3175X CPU for  $N \approx 100$ . MatDIFFNet is trained on 8 NVIDIA H800 80GB GPUs with Intel Xeon (Skylake, IBRS) 16-core CPU. All evaluations are conducted on a single RTX3090 GPU with AMD 3970X 32-Core CPU.

**Training data generation.** The train data cover four CO problems: non-metric Asymmetric TSP (ATSP), 2D Euclidean TSP (abbr. 2DTSP, metric and symmetric), Directed HCP (DHCP), and 3SAT, all in their general TSP matrix formulation. Then we generate the training data for different problems by the following protocols: **i) For ATSP, 2DTSP, and HCP**, we first randomly choose the number of nodes  $N$  from  $[\text{min\_scale}, \text{max\_scale}]$ . Then **ii) For ATSP**, we generate the distance matrix  $\mathbf{C}$  from the distribution in  $\text{Uniform}(0, 1)$  with the diagonal entries being 0; **iii) For 2DTSP**, we assign each node a random 2D coordinate by distribution  $\text{Uniform}(0, 1) \times \text{Uniform}(0, 1)$  and then compute the Euclidean distance matrix  $\mathbf{C}$ ; **iv) For DHCP**, we generate a node sequence  $\tau = (i_1, i_2, \dots, i_N)$  by randomly permuting all the nodes and assigning  $\mathbf{C}_{i_n, i_{n+1}} = 0$  for nodes in  $\tau$  and  $\mathbf{C}_{i_N, i_1} = 0$ , thus ensuring a Hamiltonian cycle in  $\mathbf{C}$ . Then we pick a random amount of node pairs  $(i, j)$  and set  $\mathbf{C}_{ij} = 0$  as the noise edge. Finally we set all  $\mathbf{C}_{ij} = 1$  for the rest node pairs  $(i, j)$ . **v) For 3SAT**, the TSP instance scale  $N$  is tied to the number of variables and clauses (Appendix A.2), so we cannot set  $N$  to an arbitrary value. We first pick a set of variable number  $N_v$  and clause number  $N_c$  as specified in Appendix D.2 to ensure that the scale of the reduced TSP instance fits different experimental scales. Finally, the instances are transformed to the general TSP form, as described in Sec. 3.2.

**Testing data preparation.** Due to the absence of previous work to standardize the evaluation of matrix-formatted general TSP across various problem distributions, we prepare 10K test instances for 3 scales (conforming to mainstream works of the ‘‘multi-task’’ concentration, see Table 6 in Appendix B.4), comprising 2,500 instances featuring each problem (ATSP, 2DTSP, HCP and 3SAT) in the matrix formulation, in pursuit of comprehensive examination across general TSP tasks.

Table 2: Main experimental results. Reported data for ATSP and 2DTSP are tour length. “Single”: models trained and tested on each problem respectively. “Mixed”: unified models trained with a mixture of 4 tasks on each scale. Asterisk (\*): a unified model trained with a mixture of 4 tasks and 3 scales. **Bold**: the best result of neural solvers. Underlined: the reference results for computing the optimality gap. **Red / blue** boxes: ours that outperform LKH with 10K/500 trials respectively. **Time**: the average time (seconds) per instance solving over each line, with batch size set to 1.

Methods	Train Data	ATSP $\downarrow$	2DTSP $\downarrow$	DHCP (L $\downarrow$ , FR $\uparrow$ )	3SAT (L $\downarrow$ , FR $\uparrow$ )	Avg. L $\downarrow$	Avg. Gap $\downarrow$	Avg. FR $\uparrow$	Time			
Scale: $N \approx 20$	Gurobi	-	1.5349	3.8347	0.0000	100.00%	0.0000	100.00%	<u>1.3424</u>	-	100.00%	<u>0.135</u>
	LKH (10000)	-	1.5349	3.8347	0.0008	99.92%	0.0000	100.00%	1.3426	0.01%	99.96%	<u>0.327</u>
	LKH (500)	-	1.5349	3.8347	0.0056	99.44%	0.0000	100.00%	1.3438	0.11%	99.72%	<u>0.038</u>
	Nearest Neighbor	-	2.0069	4.5021	3.8556	0.48%	3.0504	0.32%	3.3428	149.02%	0.40%	<u>0.000</u>
	Farthest Insertion	-	1.7070	3.9695	3.3136	1.76%	4.8816	0.00%	3.4679	158.34%	0.88%	<u>0.000</u>
	MatNet	ATSP	1.5871	4.2612	2.9608	1.12%	3.4772	0.56%	3.0716	128.82%	0.84%	<u>0.005</u>
	MatNet	Mixed	1.6359	3.9114	0.9740	27.60%	3.4656	11.04%	2.4967	85.99%	19.32%	<u>0.005</u>
	MatNet-8x	Mixed	1.5645	3.8478	0.1936	80.92%	1.6272	1.36%	1.8083	34.71%	41.14%	<u>0.037</u>
	DIMES	Mixed	2.2335	4.1696	2.9448	2.67%	2.6660	2.12%	3.0035	123.74%	2.39%	<u>0.035</u>
	DIMES-AS(100)	Mixed	1.6790	3.9092	0.4596	60.12%	0.2828	77.12%	1.5826	17.90%	68.62%	<u>0.522</u>
MatPOENet	Mixed	1.6445	3.8643	0.8676	32.60%	0.4540	61.88%	1.7076	27.21%	47.24%	<u>0.006</u>	
MatPOENet-8x	Mixed	1.5695	3.8389	0.1760	82.68%	0.0112	98.88%	1.3989	4.21%	90.78%	<u>0.043</u>	
MatPOENet*-8x	Mixed	<b>1.5506</b>	<b>3.8372</b>	<b>0.0556</b>	<b>94.44%</b>	<b>0.0008</b>	<b>99.92%</b>	<b>1.3610</b>	<b>1.39%</b>	<b>97.18%</b>	<b>0.043</b>	
Scale: $N \approx 50$	Gurobi	-	1.5545	5.6952	0.0000	100.00%	0.0000	100.00%	<u>1.8124</u>	-	100.00%	<u>0.296</u>
	LKH (10000)	-	1.5548	5.6953	0.0000	100.00%	0.2784	74.80%	1.8821	3.85%	87.40%	<u>0.513</u>
	LKH (500)	-	1.5557	5.6964	0.0000	100.00%	0.4796	61.80%	1.9329	6.65%	80.90%	<u>0.059</u>
	Nearest Neighbor	-	2.0945	6.9977	5.1120	0.00%	5.9872	0.00%	5.0548	178.90%	0.00%	<u>0.000</u>
	Farthest Insertion	-	1.8387	6.0998	4.0224	5.28%	10.3964	0.00%	5.5893	208.39%	2.64%	<u>0.001</u>
	MatNet	ATSP	1.5753	7.3618	1.4856	11.80%	8.4020	0.00%	4.7062	159.67%	5.90%	<u>0.007</u>
	MatNet	Mixed	1.8098	6.0000	0.9288	30.84%	1.1900	30.52%	2.4821	36.95%	30.68%	<u>0.007</u>
	MatNet-8x	Mixed	1.7340	5.8664	0.3056	71.52%	0.2992	73.08%	2.0513	13.18%	72.30%	<u>0.064</u>
	GLOP	Single	1.8885	6.6499	3.7244	0.84%	4.9816	0.76%	4.3111	137.87%	0.80%	<u>0.115</u>
	DIMES	Mixed	2.3341	6.6271	3.1788	1.56%	5.3656	0.12%	4.3764	141.47%	0.84%	<u>0.055</u>
DIMES-AS(100)	Mixed	1.6920	5.9447	0.5908	46.04%	1.5830	20.44%	2.4528	35.33%	33.24%	<u>2.016</u>	
MatPOENet-8x	Single	<b>1.5643</b>	<b>5.7042</b>	0.0652	93.52%	<b>0.1888</b>	<b>81.72%</b>	<b>1.8806</b>	<b>3.76%</b>	<b>87.62%</b>	<b>0.066</b>	
MatPOENet	Mixed	1.6881	5.7694	0.1444	86.20%	1.3644	27.08%	2.2416	23.68%	56.64%	<u>0.009</u>	
MatPOENet-8x	Mixed	1.6417	5.7283	<b>0.0172</b>	<b>98.28%</b>	<b>0.2456</b>	<b>77.60%</b>	<b>1.9082</b>	<b>5.29%</b>	<b>87.94%</b>	<b>0.067</b>	
MatPOENet*-8x	Mixed	1.6285	5.7575	0.0280	97.20%	0.1172	88.44%	1.8828	3.88%	<b>92.82%</b>	<b>0.067</b>	
MatDIFFNet	Single	2.0713	5.7954	2.0992	15.32%	<b>0.0464</b>	<b>98.16%</b>	2.5031	38.11%	56.74%	<u>0.157</u>	
MatDIFFNet-2OPT	Single	1.7186	5.7279	0.8324	44.08%	<b>0.0188</b>	<b>98.64%</b>	2.0744	14.46%	71.36%	<u>0.165</u>	
MatDIFFNet	Mixed	1.8385	6.2332	2.0648	15.76%	0.1112	94.68%	2.5619	41.35%	55.22%	<u>0.155</u>	
MatDIFFNet-2OPT	Mixed	1.6591	5.8619	0.8192	44.52%	0.0496	95.64%	2.0975	15.73%	70.08%	<u>0.164</u>	
Scale: $N \approx 100$	Gurobi	-	1.5661	7.7619	0.0000	100.00%	0.0000	100.00%	<u>2.3320</u>	-	100.00%	<u>0.689</u>
	LKH (10000)	-	1.5674	7.7709	0.0000	100.00%	1.0008	44.80%	2.5848	10.84%	72.40%	<u>0.811</u>
	LKH (500)	-	1.5704	7.8015	0.0000	100.00%	1.6656	28.08%	2.7594	18.33%	64.04%	<u>0.095</u>
	Nearest Neighbor	-	2.1321	9.6696	5.4016	0.20%	8.3236	0.00%	6.3859	173.84%	0.10%	<u>0.002</u>
	Farthest Insertion	-	1.9333	8.4847	3.1256	26.64%	23.5160	0.00%	9.2649	297.29%	13.32%	<u>0.003</u>
	MatNet	ATSP	<b>1.6217</b>	19.0644	17.8620	0.00%	40.1188	0.00%	19.6667	743.34%	0.00%	<u>0.015</u>
	MatNet	Mixed	1.9849	8.2551	0.9776	31.68%	2.0408	13.84%	3.3146	42.14%	22.76%	<u>0.018</u>
	MatNet-8x	Mixed	1.9210	8.1028	0.3640	69.60%	0.7740	50.76%	2.7904	19.66%	60.18%	<u>0.095</u>
	GLOP	Single	1.8491	8.8849	2.7850	2.00%	6.4280	0.08%	4.9868	113.84%	1.04%	<u>0.176</u>
	DIMES	Mixed	2.5186	9.5777	3.8064	1.16%	3.8064	0.00%	6.4018	174.52%	0.58%	<u>0.124</u>
DIMES-AS(100)	Mixed	1.6968	8.3390	0.8480	24.00%	2.8040	7.16%	3.4220	46.74%	15.58%	<u>8.437</u>	
MatPOENet	Mixed	1.9183	8.2987	0.0984	90.28%	<b>1.0704</b>	<b>32.32%</b>	2.8465	22.06%	61.30%	<u>0.017</u>	
MatPOENet-8x	Mixed	1.8655	8.1719	0.0052	99.48%	0.2440	77.12%	2.5717	10.28%	<b>88.30%</b>	<u>0.094</u>	
MatPOENet*-8x	Mixed	1.7607	8.0817	<b>0.0012</b>	<b>99.88%</b>	<b>0.3244</b>	<b>70.92%</b>	<b>2.5420</b>	<b>9.01%</b>	<b>85.40%</b>	<b>0.095</b>	
MatDIFFNet	Single	1.9432	7.9684	4.4536	2.96%	0.0404	98.44%	3.6014	54.43%	50.70%	<u>0.103</u>	
MatDIFFNet-2OPT	Single	1.7165	<b>7.8482</b>	1.1404	37.72%	<b>0.0240</b>	<b>98.60%</b>	2.6823	15.02%	68.16%	<u>0.112</u>	
MatDIFFNet	Mixed	1.8763	8.9030	3.2524	5.68%	0.1940	90.52%	3.5564	52.50%	48.10%	<u>0.102</u>	
MatDIFFNet-2OPT	Mixed	1.6965	8.1804	0.9148	43.04%	0.0952	91.44%	2.7217	16.71%	67.24%	<u>0.114</u>	

**Metrics.** **Found Rate (FR)**: the percentage of optimal solutions found in the test instances for the decisive problems HCP and SAT. A higher found rate indicates better performance. We also report the the average FR (**Avg. FR**) of DHCP and 3SAT. **Tour Length (L)**: This is the conventional metric for any TSP. The lower length indicate the better performance of the general TSP solver. We report the average tour length (**Avg. L**) over all the instances of different problem distributions. The average gap (**Avg. Gap**) is the performance drop from Gurobi w.r.t the mean tour length across the four tasks.

**Compared methods.** **Exact solver: Gurobi.** Note that the current Concorde only fits Euclidean TSP. **Heuristics: LKH** (500 and 10,000 trials), **Nearest Neighbor**, and **Farthest Insertion**. **Neural solvers: Vanilla MatNet** (Kwon et al., 2021), **DIMES** (Qiu et al., 2022) (Trained under RedCO. DIMES-AS( $T$ ) means tuned heatmap by  $T$  steps of active search, detailed in Appendix E.1), **GLOP** (Ye et al., 2024b) (using vanilla MatNet as local reviser under GLOP framework). ATSP results of **BQ-NCO** (Drakulic et al., 2023) and **GOAL** (Drakulic et al., 2024) are put in Appendix F.7 for reference only (estimated by their reported optimality gap as they are not open-sourced). **MatPOENet** (ours) and **MatDIFFNet** (ours) w/ and w/o post-inference improvements (8x parallel running for MatPOENet and 2OPT for MatDIFFNet). All evaluated neural methods are re-trained and tested on our unified dataset for fair comparison. Parameter settings are listed in Appendix D.1. Note that for HCP and SAT problems, previous specific models performed on totally different problem



432 formulation, thus orthogonal to our target of general matrix encoding TSP solving pipeline and are  
 433 reasonably excluded from evaluation in this paper. Detailed clarification of this issue is sincerely  
 434 explained in Appendix B.6 for possible concerns.

## 435 5.2 RESULTS AND DISCUSSIONS

436 Main results are shown in Table 2. In the following part, RQ1-RQ3 discuss the eternal topics of  
 437 performance, efficiency, and scalability; RQ4 analyzes the ablations upon the POE embedding;  
 438 RQ5-RQ7 introduce different applications and additional experiments based on RedCO.  
 439

440 **RQ1: Performance.** MatPOENet outperforms LKH when  $N \approx 50$  and 100 on the average length of  
 441 the full dataset. Outperforming LKH on TSP has been a pursuit by neural CO solver for long, while  
 442 scarcely are there methods achieving it, let alone on the problem of general TSP. As highlighted in  
 443 Table 2, on the scale  $N \approx 50$ , MatPOENet\* achieves to outperform LKH with max\_trials=500 on the  
 444 Avg. L i.e., the overall performance, and on the scale  $N \approx 100$ , MatPOENet\* outperforms LKH with  
 445 as many trials as max\_trials=10,000 on the Avg. L metric. *The competent results compared with LKH*  
 446 *indicates that our method MatPOENet\* can not only serve as a strong baseline for future research,*  
 447 *but also becomes a current SOTA over the problem of general TSP.* Diving deeper into the results, we  
 448 observe that LKH performs stably well on general TSP instances in continuous data space (ATSP  
 449 and 2DTSP) but is not always that good in discrete data space: It may be because of the crash of the  
 450 inherent so-called “alpha-measure” of LKH, which relies on the computing of minimum 1-tree that is  
 451 not unique in the discrete cases. [We detail the observation and analyses for LKH in Appendix G.1.](#)  
 452 The discovery of LKH’s crash also suggests the significance of developing neural solvers for general  
 453 TSP that can work simultaneously on the instances in both continuous and discrete spaces.

454 **RQ2: Efficiency.** We extract the total solving time in Table 3 for a clearer comparison. On  $N \approx 50$   
 455 data, MatPOENet achieves better tour length (1.91 v.s. 1.93) within shorter time (7m31s v.s. 9m9s)  
 456 compared to LKH-500. More impressively, on  $N \approx 100$  data, MatPOENet not only beats LKH-500  
 457 on both run-time efficiency and average quality, but also show superiority in solving performance (2.57  
 458 v.s. 2.58) compared to LKH-10000 which consumes 8.7x time (15m35s v.s. 2h15m). MatDIFFNet  
 459 consumes more solving time for its complex inference denoising steps of diffusion, yet also reaches  
 460 competitive results against LKH within a similar solving time.

461 Table 3: Results of both solving time and solving quality comparing Mat-X-Net (ours) and different  
 462 settings of LKH. LKH-N: LKH with 1 runs and N max\_trials. Batch size = 1.

	Method	Time↓	ATSP↓	2DTSP↓	DHCP (L↓, FR↑)		3SAT (L↓, FR↑)		Avg. L↓
$N \approx 50$	MatPOENet	7m31s	1.6417	5.7283	0.0172	98.28%	0.2456	77.60%	1.9082
	MatDIFFNet	21m48s	1.7186	5.7279	0.8324	44.08%	0.0188	98.64%	2.0744
	LKH-500	9m9s	1.5557	5.6964	0.0000	100.00%	0.4796	61.80%	1.9329
	LKH-1000	13m53s	1.5554	5.6957	0.0000	100.00%	0.4160	65.68%	1.9168
	LKH-10000	1h22m	1.5548	5.6953	0.0000	100.00%	0.2784	74.80%	1.8821
$N \approx 100$	MatPOENet	15m35s	1.8655	8.1719	0.0052	99.48%	0.2440	77.12%	2.5717
	MatDIFFNet	28m21s	1.7165	7.8482	1.1404	37.72%	0.0240	98.60%	2.6823
	LKH-500	15m49s	1.5704	7.8015	0.0000	100.00%	1.6656	28.08%	2.7594
	LKH-1000	24m39s	1.5692	7.7909	0.0000	100.00%	1.4400	32.52%	2.7000
	LKH-10000	2h15m	1.5674	7.7709	0.0000	100.00%	1.0008	44.80%	2.5848

472 **RQ3: Scalability.** Experiments are conducted from three aspects to show the multi-scale general-  
 473 izeability: **i) MatPOENet trained on all the scales.** We train an MatPOENet with training data of  
 474 all the scales, denoted by MatPOENet\* in Table 2. Competitive results are obtained compared to  
 475 single training, demonstrating the feasibility of, and even benefits brought by multi-scale training. **ii)**  
 476

477 Table 4: Case study of  $N > d$ :  $d_1 = 512$ ,  $d_2 = 32$  on the scale  $N \approx 50$ .

Method	ATSP↓	2DTSP↓	DHCP (L↓, FR↑)		3SAT(L↓, FR↑)		Avg. L↓
MatPOENet ( $N \ll d_1$ )	1.6417	5.7283	0.0172	98.28%	0.2456	77.60%	1.9082
MatPOENet ( $N > d_2$ )	1.8799	5.9742	0.4548	60.24%	0.3292	75.56%	2.1595

481 **Scale-free initializer POE on the scale  $N > d$ .** In response to the motivation of designing POE  
 482 in Sec. 4.2.1, we show that MatPOENet can be trained on instances at the scale  $N$  larger than the  
 483 pre-set one-hot embedding dimension  $d$ , which is the case where vanilla MatNet fails. Results in the  
 484 case  $N > d$  are given in Table 4. Compared with the model trained with a higher  $d$ , we observe that  
 485 a reduced  $d$  would cause a reasonable degeneracy of model performance. **iii) On larger-scaled data.**  
 In terms of solving large scaled CO problems, resorting to divide-and-conquer paradigm is popular

and proved feasible and performant (Ye et al., 2024b; Luo et al., 2024; Fu et al., 2021), where a strong solver at small-to-medium instances is still of irreplaceable importance. We readily incorporated the state-of-the-art GLOP (Ye et al., 2024b) which greatly improves MatNet’s scalability. Results of the GLOP-empowered MatPOENet (Ours) are presented below, which can be regarded as an initial indication for the efficiency of our proposed POE at large scaled problems (128 instances for  $N = 1K$  and 16 instances for  $N = 10K$ ). Note BiTSP is a direct simulation of decisive CO problems in general TSP formulation, referring to randomly generated instances that has binary distances but does not necessarily possess a zero-length loop. A more thorough discussion of scalability and applicability issues from the view of current research status of unified NCO is deferred to Appendix G.2.

Table 5: Results on large-scaled ATSP instances.

Scale	Method	ATSP (L↓)	Time	BiTSP (L↓)	Time	HCP (L↓)	FR↑	Time
1K	Greedy	2.146	21s	5.609	21s	5.734	0.00%	21s
	MatNet	2.130	1m24s	4.352	1m	3.063	0.78%	45s
	Ours	<b>2.092</b>	<b>57s</b>	<b>0.517</b>	<b>40s</b>	<b>0.563</b>	<b>64.84%</b>	<b>41s</b>
10K	Greedy	9.516	4m32s	5.938	4m32s	5.438	0.00%	4m32s
	MatNet	9.184	23m17s	3.313	6m10s	2.750	0.00%	23m22s
	Ours	<b>8.355</b>	<b>5m27s</b>	<b>0.688</b>	<b>5m10s</b>	<b>0.625</b>	<b>62.50%</b>	<b>5m40s</b>

**RQ4: Ablations of POE (Appendix F.1).** i) **MatNet v.s. MetPOENet.** Main results in Table 2 validate the effectiveness of introducing POE to enhance MatNet. ii) **Comparison of different initial rough solver.** Results of nearest neighbor (NN), farthest insertion (FI), and an ablation without rough solvers (Non) in Table 10 show superiority of NN as the initial solver for POE. We speculate that it is because NN pays more attention to the local structure, complementing subsequent attention layers where global information are learned. iii) **POE v.s. alternatives.** Fixed random vectors and trainable embeddings are tested as the substitution of the proposed POE. Results in Table 11 show that our POE outperforms the other two options suggested in the paper of MatNet (Kwon et al., 2021).

**RQ5: RedCO for Pretraining-Finetuning (Appendix F.2).** With MatPOENet, RedCO executes both i) **cross-task** and ii) **cross-scale** experiments for pretraining-finetuning applications. With MatDIFFNet, RedCO also trains the model in the curriculum learning manner, i.e., models on larger scales are trained upon existing weights gained during training of small scaled data. Results in Appendix F.2 demonstrate applicability of RedCO as a pretraining-finetuning framework.

**RQ6: RedCO for Other Learning Paradigms and Problems. (Appendix F.3 & F.4).** Besides aforementioned methods (DRL, Generative, etc.), RedCO is also available for the mainstream supervised learning (SL) of neural heatmap for general TSP solving. We perform minimum modification to the backbone model in MatPOENet to obtain a heatmap predictor via pure supervised learning. Results are provided in Appendix F.3 Also, supplementary experiments on the vertex cover problem (VC) have been conducted using RedCO. Results and discussions are in F.4. To conclude, RedCO along with our Mat-X-Nets possess good adaptability to embrace new learning paradigms and tasks.

**RQ7: RedCO for standard TSP and Real-world Generalization (Appendix F.5 & F.6).** In order to reach better alignment to previous works that focused on 2DTSP only, we have conducted experiments on the standard test set shared by a series typical works (Kool et al., 2018; Joshi et al., 2019; Min et al., 2024; Qiu et al., 2022; Li et al., 2023; Hudson et al., 2021), with 1280 instances each for TSP-50 and TSP-100. Also, we test MatPOENet and MatDIFFNet on 45 selected real-world instances ( $N \in [14, 195]$ ) from the well-kown TSPLIB. Results (in Table 18, 19, 21, respectively) demonstrate that our designed networks manage to solve the conventional Euclidean TSPs without coordination as input, yielding comparable performance and generalizability.

## 6 CONCLUSION AND FUTURE WORK

**Conclusion.** In this paper, we first propose the RedCO framework to embed different CO problems in a consistent general TSP matrix format via problem reduction. Further, we delve into the under-explored realm of matrix-formulated TSP and devise MatPOENet and MatDIFFNet as plugs-in of RedCO, in aid of current lack of neural capability targeting general TSP.

**Limitations and Future Work.** We have made an initial step towards the general neural CO solver. Future works include: i) **More problems.** More CO problems reducible to general TSP (Appendix E.2) shall be included for evaluation. ii) **Stronger capability.** Gaps still exist comparing to exact solvers at specific problem solving. iii) **Better scalability.** MatDIFFNet has the potential to scale larger and work as a consistency model in the future (Appendix G.4).

## 540 ETHICS STATEMENT

541

542 The methods proposed in this paper aim to improve the field of neural CO solver with better generality.  
 543 A dataset comprising synthetic instances of general TSPs with different problem distributions will be  
 544 released upon publication, to facilitate the under-studied branch of matrix-formulated TSP thereby  
 545 broadening the scope of evaluation of the ML4TSP and even the ML4CO community. To our best  
 546 knowledge, no potential harmful insights of this work that need to be otherwise stated.

547

## 548 REPRODUCIBILITY STATEMENT

549

550 The hardware and the preparation of the used data are described in Sec. 5.1. The detailed parameteri-  
 551 zation and implementation of the models for training and testing are provided in Appendix D. Source  
 552 code and datasets shall be open-sourced after the review process.

553

## 554 REFERENCES

555

556 Saeed Amizadeh, Sergiy Matushevych, and Markus Weimer. Learning to solve circuit-sat: An  
 557 unsupervised differentiable approach. In *International Conference on Learning Representations*,  
 558 2018.

559 Saeed Amizadeh, Sergiy Matushevych, and Markus Weimer. Pdp: A general neural framework for  
 560 learning constraint satisfaction solvers. *arXiv preprint arXiv:1903.01969*, 2019.

561

562 Jacob Austin, Daniel D. Johnson, Jonathan Ho, Daniel Tarlow, and Rianne van den Berg. Structured  
 563 denoising diffusion models in discrete state-spaces, 2023. URL [https://arxiv.org/abs/  
 564 2107.03006](https://arxiv.org/abs/2107.03006).

565 Irwan Bello, Hieu Pham, Quoc V Le, Mohammad Norouzi, and Samy Bengio. Neural combinatorial  
 566 optimization with reinforcement learning. *arXiv preprint arXiv:1611.09940*, 2016.

567

568 Federico Berto, Chuanbo Hua, Junyoung Park, Laurin Luttmann, Yining Ma, Fanchen Bu, Jiarui  
 569 Wang, Haoran Ye, Minsu Kim, Sanghyeok Choi, Nayeli Gast Zepeda, André Hottung, Jianan  
 570 Zhou, Jieyi Bi, Yu Hu, Fei Liu, Hyeonah Kim, Jiwoo Son, Haeyeon Kim, Davide Angioni,  
 571 Wouter Kool, Zhiguang Cao, Qingfu Zhang, Joungho Kim, Jie Zhang, Kijung Shin, Cathy Wu,  
 572 Sungsoo Ahn, Guojie Song, Changhyun Kwon, Kevin Tierney, Lin Xie, and Jinkyoo Park. RL4co:  
 573 an extensive reinforcement learning for combinatorial optimization benchmark, 2024. URL  
 574 <https://arxiv.org/abs/2306.17100>.

575 Léo Boisvert, H el ene Verhaeghe, and Quentin Cappart. Towards a generic representation of com-  
 576 binatorial problems for learning-based approaches, 2024. URL [https://arxiv.org/abs/  
 577 2403.06026](https://arxiv.org/abs/2403.06026).

578 Xavier Bresson and Thomas Laurent. An experimental study of neural networks for variable graphs.  
 579 *ICLR workshop*, 2018.

580

581 Chris Cameron, Rex Chen, Jason Hartford, and Kevin Leyton-Brown. Predicting propositional satis-  
 582 fiability via end-to-end learning. In *Proceedings of the AAAI Conference on Artificial Intelligence*,  
 583 volume 34, pp. 3324–3331, 2020.

584 Paulo R d O da Costa, Jason Rhuggenaath, Yingqian Zhang, and Alp Akcay. Learning 2-opt  
 585 heuristics for the traveling salesman problem via deep reinforcement learning. In Sinno Jialin Pan  
 586 and Masashi Sugiyama (eds.), *Proceedings of The 12th Asian Conference on Machine Learning*,  
 587 volume 129 of *Proceedings of Machine Learning Research*, pp. 465–480. PMLR, 18–20 Nov 2020.  
 588 URL <https://proceedings.mlr.press/v129/costa20a.html>.

589 Darko Drakulic, Sofia Michel, Florian Mai, Arnaud Sors, and Jean-Marc Andreoli. Bq-nco:  
 590 Bisimulation quotienting for efficient neural combinatorial optimization, 2023. URL <https://arxiv.org/abs/2301.03313>.

591

592 Darko Drakulic, Sofia Michel, and Jean-Marc Andreoli. Goal: A generalist combinatorial optimiza-  
 593 tion agent learner, 2024. URL <https://arxiv.org/abs/2406.15079>.

- 594 Stefan Elfving, Eiji Uchibe, and Kenji Doya. Sigmoid-weighted linear units for neural network  
595 function approximation in reinforcement learning. *Neural networks*, 107:3–11, 2018.  
596
- 597 Eric Fouh, Ville Karavirta, Daniel A Breakiron, Sally Hamouda, Simin Hall, Thomas L Naps, and  
598 Clifford A Shaffer. Design and architecture of an interactive etextbook—the opensa system.  
599 *Science of computer programming*, 88:22–40, 2014.
- 600 Zhang-Hua Fu, Kai-Bin Qiu, and Hongyuan Zha. Generalize a small pre-trained model to arbitrarily  
601 large tsp instances. In *Proceedings of the AAAI conference on artificial intelligence*, volume 35,  
602 pp. 7474–7482, 2021.  
603
- 604 Wenxuan Guo, Hui-Ling Zhen, Xijun Li, Wanqian Luo, Mingxuan Yuan, Yaohui Jin, and Junchi  
605 Yan. Machine learning methods in solving the boolean satisfiability problem. *Machine Intelligence*  
606 *Research*, 20(5):640–655, June 2023. ISSN 2731-5398. doi: 10.1007/s11633-022-1396-2. URL  
607 <http://dx.doi.org/10.1007/s11633-022-1396-2>.
- 608 LLC Gurobi Optimization. Gurobi optimizer reference manual. *Gurobi*, pp. 2–12, 2021.  
609
- 610 Michael Hahsler and Kurt Hornik. Tsp-infrastructure for the traveling salesperson problem. *Journal*  
611 *of Statistical Software*, 23(2):1–21, 2007.  
612
- 613 Keld Helsgaun. An extension of the lin-kernighan-helsgaun tsp solver for constrained traveling  
614 salesman and vehicle routing problems. *Roskilde: Roskilde University*, 12, 2017.
- 615 Jonathan Ho, Ajay Jain, and Pieter Abbeel. Denoising diffusion probabilistic models, 2020. URL  
616 <https://arxiv.org/abs/2006.11239>.  
617
- 618 André Hottung, Bhanu Bhandari, and Kevin Tierney. Learning a latent search space for routing  
619 problems using variational autoencoders. In *International Conference on Learning Representations*,  
620 2021a.
- 621 André Hottung, Yeong-Dae Kwon, and Kevin Tierney. Efficient active search for combinatorial  
622 optimization problems. *arXiv preprint arXiv:2106.05126*, 2021b.  
623
- 624 Benjamin Hudson, Qingbiao Li, Matthew Malencia, and Amanda Prorok. Graph neural network  
625 guided local search for the traveling salesperson problem. *arXiv preprint arXiv:2110.05291*, 2021.  
626
- 627 Sebastian Jaszczur, Michał Łuszczczyk, and Henryk Michalewski. Neural heuristics for sat solving.  
628 *arXiv preprint arXiv:2005.13406*, 2020.
- 629 Xia Jiang, Yaoxin Wu, Yuan Wang, and Yingqian Zhang. Unco: Towards unifying neural combina-  
630 torial optimization through large language model, 2024. URL [https://arxiv.org/abs/](https://arxiv.org/abs/2408.12214)  
631 [2408.12214](https://arxiv.org/abs/2408.12214).  
632
- 633 Chaitanya K Joshi, Thomas Laurent, and Xavier Bresson. An efficient graph convolutional network  
634 technique for the travelling salesman problem. *arXiv preprint arXiv:1906.01227*, 2019.
- 635 Chaitanya K. Joshi, Quentin Cappart, Louis-Martin Rousseau, and Thomas Laurent. Learning the  
636 travelling salesperson problem requires rethinking generalization. *arXiv preprint arXiv:2006.07054*,  
637 2020.  
638
- 639 Richard M. Karp. *Reducibility among Combinatorial Problems*, pp. 85–103. Springer US, Boston,  
640 MA, 1972. ISBN 978-1-4684-2001-2. doi: 10.1007/978-1-4684-2001-2\_9. URL [https://](https://doi.org/10.1007/978-1-4684-2001-2_9)  
641 [doi.org/10.1007/978-1-4684-2001-2\\_9](https://doi.org/10.1007/978-1-4684-2001-2_9).
- 642 Elias Khalil, Hanjun Dai, Yuyu Zhang, Bistra Dilikina, and Le Song. Learning combinatorial  
643 optimization algorithms over graphs. *Advances in neural information processing systems*, 30,  
644 2017.  
645
- 646 Minsu Kim, Junyoung Park, and Jinkyoo Park. Sym-nco: Leveraging symmetry for neural  
647 combinatorial optimization. *Advances in Neural Information Processing Systems*, 35:1936–1949,  
2022.

- 648 Minsu Kim, Sanghyeok Choi, Jiwoo Son, Hyeonah Kim, Jinkyoo Park, and Yoshua Bengio. Ant  
649 colony sampling with gflownets for combinatorial optimization. *arXiv preprint arXiv:2403.07041*,  
650 2024.
- 651 DP Kingma. Adam: a method for stochastic optimization. In *Int Conf Learn Represent*, 2014.
- 652 Thomas N Kipf and Max Welling. Semi-supervised classification with graph convolutional networks.  
653 *arXiv preprint arXiv:1609.02907*, 2016.
- 654 Wouter Kool, Herke Van Hoof, and Max Welling. Attention, learn to solve routing problems! *arXiv*  
655 *preprint arXiv:1803.08475*, 2018.
- 656 Wouter Kool, Herke van Hoof, and Max Welling. Buy 4 reinforce samples, get a baseline for free!  
657 2019.
- 658 Wouter Kool, Herke van Hoof, Joaquim Gromicho, and Max Welling. Deep policy dynamic pro-  
659 gramming for vehicle routing problems. In *International conference on integration of constraint*  
660 *programming, artificial intelligence, and operations research*, pp. 190–213. Springer, 2022.
- 661 Yeong-Dae Kwon, Jinho Choo, Byoungjip Kim, Iljoo Yoon, Youngjune Gwon, and Seungjai Min.  
662 Pomo: Policy optimization with multiple optima for reinforcement learning. *Advances in Neural*  
663 *Information Processing Systems*, 33:21188–21198, 2020.
- 664 Yeong-Dae Kwon, Jinho Choo, Iljoo Yoon, Minah Park, Duwon Park, and Youngjune Gwon. Ma-  
665 trix encoding networks for neural combinatorial optimization. *Advances in Neural Information*  
666 *Processing Systems*, 34:5138–5149, 2021.
- 667 Harry R Lewis. Michael r. πgarey and david s. johnson. computers and intractability. a guide to the  
668 theory of np-completeness. wh freeman and company, san francisco1979, x+ 338 pp. *The Journal*  
669 *of Symbolic Logic*, 48(2):498–500, 1983.
- 670 Peng Li and Bo Liu. Multi-task combinatorial optimization: Adaptive multi-modality knowledge  
671 transfer by an explicit inter-task distance. *arXiv preprint arXiv:2305.12807*, 2023.
- 672 Yang Li, Jinpei Guo, Runzhong Wang, and Junchi Yan. From distribution learning in training  
673 to gradient search in testing for combinatorial optimization. In *Thirty-seventh Conference on*  
674 *Neural Information Processing Systems*, 2023. URL [https://openreview.net/forum?](https://openreview.net/forum?id=JtF0ugNMv2)  
675 [id=JtF0ugNMv2](https://openreview.net/forum?id=JtF0ugNMv2).
- 676 Zhaoyu Li and Xujie Si. Nsnet: A general neural probabilistic framework for satisfiability problems.  
677 *Advances in Neural Information Processing Systems*, 35:25573–25585, 2022.
- 678 Fei Liu, Xi Lin, Zhenkun Wang, Qingfu Zhang, Xialiang Tong, and Mingxuan Yuan. Multi-  
679 task learning for routing problem with cross-problem zero-shot generalization, 2024. URL  
680 <https://arxiv.org/abs/2402.16891>.
- 681 Ilya Loshchilov and Frank Hutter. Decoupled weight decay regularization. In *International Confer-*  
682 *ence on Learning Representations*, 2018.
- 683 Fu Luo, Xi Lin, Zhenkun Wang, Xialiang Tong, Mingxuan Yuan, and Qingfu Zhang. Self-improved  
684 learning for scalable neural combinatorial optimization, 2024. URL [https://arxiv.org/](https://arxiv.org/abs/2403.19561)  
685 [abs/2403.19561](https://arxiv.org/abs/2403.19561).
- 686 Yining Ma, Zhiguang Cao, and Yeow Meng Chee. Learning to search feasible and infeasible regions  
687 of routing problems with flexible neural k-opt. In *Thirty-seventh Conference on Neural Information*  
688 *Processing Systems*, 2023. URL <https://openreview.net/forum?id=q1JukwH2yP>.
- 689 Yimeng Min, Frederik Wenkel, and Guy Wolf. Geometric scattering attention networks. In *ICASSP*  
690 *2021 - 2021 IEEE International Conference on Acoustics, Speech and Signal Processing (ICASSP)*.  
691 IEEE, June 2021. doi: 10.1109/icassp39728.2021.9414557. URL [http://dx.doi.org/10.](http://dx.doi.org/10.1109/ICASSP39728.2021.9414557)  
692 [1109/ICASSP39728.2021.9414557](http://dx.doi.org/10.1109/ICASSP39728.2021.9414557).
- 693 Yimeng Min, Yiwei Bai, and Carla P. Gomes. Unsupervised learning for solving the travelling  
694 salesman problem, 2024. URL <https://arxiv.org/abs/2303.10538>.

- 702 Emils Ozolins, Karlis Freivalds, Andis Draguns, Eliza Gaile, Ronalds Zakovskis, and Sergejs  
703 Kozlovics. Goal-aware neural sat solver. In *2022 International Joint Conference on Neural  
704 Networks (IJCNN)*, pp. 1–8. IEEE, 2022.
- 705  
706 Ruizhong Qiu, Zhiqing Sun, and Yiming Yang. DIMES: A differentiable meta solver for combinatorial  
707 optimization problems. In *Advances in Neural Information Processing Systems 35*, 2022.
- 708 Sebastian Sanokowski, Wilhelm Berghammer, Sepp Hochreiter, and Sebastian Lehner. Variational  
709 annealing on graphs for combinatorial optimization. volume 36, pp. 63907–63930, 2023.
- 710  
711 Sebastian Sanokowski, Sepp Hochreiter, and Sebastian Lehner. A diffusion model framework  
712 for unsupervised neural combinatorial optimization. In *Forty-first International Conference on  
713 Machine Learning*, 2024.
- 714 Martin JA Schuetz, J Kyle Brubaker, and Helmut G Katzgraber. Combinatorial optimization with  
715 physics-inspired graph neural networks. *Nature Machine Intelligence*, 4(4):367–377, 2022.
- 716  
717 Daniel Selsam and Nikolaj Bjørner. Guiding high-performance sat solvers with unsat-core predictions.  
718 In *Theory and Applications of Satisfiability Testing–SAT 2019: 22nd International Conference,  
719 SAT 2019, Lisbon, Portugal, July 9–12, 2019, Proceedings 22*, pp. 336–353. Springer, 2019.
- 720 Daniel Selsam, Matthew Lamm, Benedikt Bünz, Percy Liang, Leonardo de Moura, and David L Dill.  
721 Learning a sat solver from single-bit supervision. *arXiv preprint arXiv:1802.03685*, 2018.
- 722  
723 Mohamed A Wahby Shalaby, Ayman R Mohammed, and Sally S Kassem. Supervised fuzzy c-means  
724 techniques to solve the capacitated vehicle routing problem. *Int. Arab J. Inf. Technol.*, 18(3A):  
725 452–463, 2021.
- 726  
727 Jiaming Song, Chenlin Meng, and Stefano Ermon. Denoising diffusion implicit models. *CoRR*,  
728 abs/2010.02502, 2020. URL <https://arxiv.org/abs/2010.02502>.
- 729 Yang Song and Prafulla Dhariwal. Improved techniques for training consistency models. In *The  
730 Twelfth International Conference on Learning Representations*.
- 731  
732 IBM ILOG CPLEX Optimization Studio. V20.1: User’s manual for cplex. *IBM Corp*, pp. 1–20,  
733 2020.
- 734 Jingyan Sui, Shizhe Ding, Rui Tao Liu, Liming Xu, and Dongbo Bu. Learning 3-opt heuristics for trav-  
735 eling salesman problem via deep reinforcement learning. In *Asian Conference on Machine Learn-  
736 ing*, 2021. URL <https://api.semanticscholar.org/CorpusID:249038331>.
- 737  
738 Jingyan Sui, Shizhe Ding, Boyang Xia, Ruizhi Liu, and Dongbo Bu. Neuralgls: learning to guide  
739 local search with graph convolutional network for the traveling salesman problem. *Neural Comput.  
740 Appl.*, 36(17):9687–9706, October 2023. ISSN 0941-0643. doi: 10.1007/s00521-023-09042-6.  
741 URL <https://doi.org/10.1007/s00521-023-09042-6>.
- 742 Zhiqing Sun and Yiming Yang. DIFUSCO: Graph-based diffusion solvers for combinatorial opti-  
743 mization. In *Thirty-seventh Conference on Neural Information Processing Systems*, 2023.
- 744  
745 Junior Mele U, Maria Gambardella L, and Montemanni R. Machine. Machine learning approaches for  
746 the traveling salesman problem: A survey. In *Proceedings of the 2021 8th International Conference  
747 on Industrial Engineering and Applications (Europe)*, 2021.
- 748 Pashootan Vaezipoor, Gil Lederman, Yuhuai Wu, Chris Maddison, Roger B Grosse, Sanjit A Se-  
749 shia, and Fahiem Bacchus. Learning branching heuristics for propositional model counting. In  
750 *Proceedings of the AAAI Conference on Artificial Intelligence*, volume 35, pp. 12427–12435, 2021.
- 751 Jan Van Leeuwen. *Handbook of theoretical computer science (vol. A) algorithms and complexity*.  
752 Mit Press, 1991.
- 753  
754 Ashish Vaswani, Noam Shazeer, Niki Parmar, Jakob Uszkoreit, Llion Jones, Aidan N Gomez, Łukasz  
755 Kaiser, and Illia Polosukhin. Attention is all you need. *Advances in neural information processing  
systems*, 30, 2017.

- 756 Oriol Vinyals, Meire Fortunato, and Navdeep Jaitly. Pointer networks. In C. Cortes,  
757 N. Lawrence, D. Lee, M. Sugiyama, and R. Garnett (eds.), *Advances in Neural In-*  
758 *formation Processing Systems*, volume 28. Curran Associates, Inc., 2015. URL  
759 [https://proceedings.neurips.cc/paper\\_files/paper/2015/file/](https://proceedings.neurips.cc/paper_files/paper/2015/file/29921001f2f04bd3baee84a12e98098f-Paper.pdf)  
760 [29921001f2f04bd3baee84a12e98098f-Paper.pdf](https://proceedings.neurips.cc/paper_files/paper/2015/file/29921001f2f04bd3baee84a12e98098f-Paper.pdf).
- 761 Chenguang Wang and Tianshu Yu. Efficient training of multi-task combinatorial neural solver with  
762 multi-armed bandits. *arXiv preprint arXiv:2305.06361*, 2023.
- 763 Chenguang Wang, Zhouliang Yu, Stephen McAleer, Tianshu Yu, and Yaodong Yang. Asp: Learn a  
764 universal neural solver! *IEEE TPAMI*, 2024.
- 765 Runzhong Wang, Zhigang Hua, Gan Liu, Jiayi Zhang, Junchi Yan, Feng Qi, Shuang Yang, Jun Zhou,  
766 and Xiaokang Yang. A bi-level framework for learning to solve combinatorial optimization on  
767 graphs. *Advances in Neural Information Processing Systems*, 34:21453–21466, 2021.
- 768 Ronald J Williams. Simple statistical gradient-following algorithms for connectionist reinforcement  
769 learning. *Machine learning*, 8:229–256, 1992.
- 770 Yifan Xia, Xianliang Yang, Zichuan Liu, Zhihao Liu, Lei Song, and Jiang Bian. Position: Rethinking  
771 post-hoc search-based neural approaches for solving large-scale traveling salesman problems, 2024.  
772 URL <https://arxiv.org/abs/2406.03503>.
- 773 Yubin Xiao, Di Wang, Boyang Li, Mingzhao Wang, Xuan Wu, Changliang Zhou, and You Zhou.  
774 Distilling autoregressive models to obtain high-performance non-autoregressive solvers for vehicle  
775 routing problems with faster inference speed, 2024. URL [https://arxiv.org/abs/2312.](https://arxiv.org/abs/2312.12469)  
776 [12469](https://arxiv.org/abs/2312.12469).
- 777 Liang Xin, Wen Song, Zhiguang Cao, and Jie Zhang. NeuroLKH: Combining deep learning model  
778 with lin-kernighan-helsgaun heuristic for solving the traveling salesman problem. In *Advances in*  
779 *Neural Information Processing Systems*, volume 34, 2021.
- 780 Haoran Ye, Jiarui Wang, Zhiguang Cao, Helan Liang, and Yong Li. Deepaco: neural-enhanced ant  
781 systems for combinatorial optimization. *Advances in Neural Information Processing Systems*, 36,  
782 2024a.
- 783 Haoran Ye, Jiarui Wang, Helan Liang, Zhiguang Cao, Yong Li, and Fanzhang Li. Glop: Learning  
784 global partition and local construction for solving large-scale routing problems in real-time. In  
785 *Proceedings of the AAAI Conference on Artificial Intelligence*, 2024b.
- 786 J Zhang, C Liu, X Li, HL Zhen, M Yuan, Y Li, and J. Yan. A survey for solving mixed integer  
787 programming via machine learning. *Neurocomputing*, 2023.
- 788 Jiongzi Zheng, Kun He, Jianrong Zhou, Yan Jin, and Chu-Min Li. Combining reinforcement learning  
789 with lin-kernighan-helsgaun algorithm for the traveling salesman problem. *Proceedings of the AAAI*  
790 *Conference on Artificial Intelligence*, 35(14):12445–12452, May 2021. doi: 10.1609/aaai.v35i14.  
791 17476. URL <https://ojs.aaai.org/index.php/AAAI/article/view/17476>.
- 792 Jianan Zhou, Zhiguang Cao, Yaoxin Wu, Wen Song, Yining Ma, Jie Zhang, and Chi Xu. Mvmoe:  
793 Multi-task vehicle routing solver with mixture-of-experts, 2024. URL [https://arxiv.org/](https://arxiv.org/abs/2405.01029)  
794 [abs/2405.01029](https://arxiv.org/abs/2405.01029).
- 800  
801  
802  
803  
804  
805  
806  
807  
808  
809

# Appendix

810  
811  
812  
813  
814  
815  
816  
817  
818  
819  
820  
821  
822  
823  
824  
825  
826  
827  
828  
829  
830  
831  
832  
833  
834  
835  
836  
837  
838  
839  
840  
841  
842  
843  
844  
845  
846  
847  
848  
849  
850  
851  
852  
853  
854  
855  
856  
857  
858  
859  
860  
861  
862  
863

## CONTENTS

<b>A</b>	<b>Details of Problem Reduction and Solution Transformation</b>	<b>18</b>
A.1	HCP v.s. TSP . . . . .	18
A.2	3SAT v.s. HCP . . . . .	18
A.2.1	Reduction from 3SAT to HCP . . . . .	18
A.2.2	Transform HCP Solution to 3SAT Solution . . . . .	19
<b>B</b>	<b>Additional Related Work</b>	<b>19</b>
B.1	Conventional Solvers . . . . .	19
B.2	Learning Methods for TSP . . . . .	19
B.3	Combination of Neural and OR Methods . . . . .	20
B.4	Multi-Task CO Models . . . . .	20
B.5	Specific Solvers for SAT and HCP . . . . .	22
B.6	Note on Evaluation of Specific Solvers . . . . .	22
<b>C</b>	<b>Network Details</b>	<b>22</b>
C.1	Vanilla MatNet and MatPOENet . . . . .	22
C.2	Graph-based Diffusion and MatDIFFNet . . . . .	24
<b>D</b>	<b>Experimental Details</b>	<b>25</b>
D.1	Hyperparameters . . . . .	25
D.2	Scale Setting of 3SAT Instances . . . . .	26
D.3	Training Curves . . . . .	26
<b>E</b>	<b>More Applications of RedCO</b>	<b>27</b>
E.1	More Adaptable Backbone: GNN-based DIMES . . . . .	27
E.1.1	Network Architecture . . . . .	28
E.1.2	Training Process . . . . .	28
E.1.3	Results and Discussion . . . . .	29
E.2	More Applicable Problems . . . . .	30
E.2.1	Vertex Cover . . . . .	30
E.2.2	Clique Problem . . . . .	30
E.2.3	Independent Set Problem . . . . .	30
E.2.4	Vehicle Routing Problems . . . . .	31
E.2.5	MatPOENet & MatDIFFNet as Problem-Specific Solver . . . . .	31
<b>F</b>	<b>Supplementary Experiments</b>	<b>31</b>
F.1	Further Experiments of POE . . . . .	31



864	F.2 Pretraining-Finetuning Applications . . . . .	32
865	F.3 Comparison of Learning Paradigms . . . . .	33
866	F.4 Results on Vertex Cover Problem . . . . .	33
867	F.5 Results on Standard Symmetric TSP . . . . .	34
868	F.6 Results on Real-world Instances . . . . .	34
869	F.7 Full Experimental Results . . . . .	35
870		
871	<b>G Further Discussions</b>	<b>35</b>
872		
873	G.1 Note on LKH . . . . .	35
874	G.2 Note on the Scalability and Applicability . . . . .	37
875	G.3 Discussion of MatPOENet v.s. MatDIFFNet . . . . .	37
876	G.4 Discussion of Generative Combinatorial Optimization . . . . .	38
877		
878		
879		
880		
881		
882		
883		
884		
885		
886		
887		
888		
889		
890		
891		
892		
893		
894		
895		
896		
897		
898		
899		
900		
901		
902		
903		
904		
905		
906		
907		
908		
909		
910		
911		
912		
913		
914		
915		
916		
917		

## A DETAILS OF PROBLEM REDUCTION AND SOLUTION TRANSFORMATION

For easy reading, here we give a review of the mathematical definitions of covered problems. Then we give the proof to problem reduction relations in the following sections.

**Definition 1** (Traveling Salesman Problem (TSP)). *Given a complete, directed or undirected graph without self-loops denoted by  $G = (\mathcal{V}, \mathcal{E})$  ( $\mathcal{V} = \{1, 2, \dots, N\}$ : the node set,  $\mathcal{E}$ : the edge set) along with a cost matrix  $\mathbf{C}$  of the shape  $N \times N$  where the entry  $\mathbf{C}_{ij}$  is the cost for edge  $(i, j) \in \mathcal{E}$ , the problem is to find the tour  $\tau = (i_1, \dots, i_N)$  to minimize the cost  $\sum_{k=1}^{N-1} \mathbf{C}_{i_k i_{k+1}} + \mathbf{C}_{i_N i_1}$ .*

**Definition 2** (Hamiltonian Cycle Problem (HCP)). *Given a directed or undirected graph  $G = (\mathcal{V}, \mathcal{E})$ , the problem is to determine whether there exists a Hamiltonian cycle in  $G$ .*

**Definition 3** (Boolean Satisfiability Problem (SAT) in conjunctive normal form (CNF)). *SAT aims to determine the existence of an interpretation that satisfies a given Boolean formula. A Boolean formula in CNF is represented by a conjunction (denoted by  $\wedge$ ) of clauses that are disjunctions (denoted by  $\vee$ ) of variables. For example,  $(x_1 \vee \neg x_2) \wedge (\neg x_1 \vee x_2 \vee \neg x_3)$  is a SAT instance of two clauses  $(x_1 \vee \neg x_2)$  and  $(\neg x_1 \vee x_2 \vee \neg x_3)$ , and three variables  $x_1, x_2$  and  $x_3$ .*

A special case of SAT in CNF where the number of variables is no more than 3 is named as 3-Satisfiability (3SAT). Note any SAT problem can be reduced to 3SAT in polynomial time (Fouh et al., 2014). So without losing generality, we pick 3SAT for evaluation.

### A.1 HCP v.s. TSP

To transform the graph  $G = (\mathcal{V}, \mathcal{E})$  of an HCP instance to the cost matrix  $\mathbf{C}$  of a TSP instance, we simply set  $\mathbf{C}_{ij} = 0$  if  $(i, j) \in \mathcal{E}$  and  $\mathbf{C}_{ij} = 1$  otherwise. Then the problem of finding a Hamiltonian cycle becomes finding a tour of length 0 (also the minimum length) for the TSP instance with cost matrix  $\mathbf{C}$ . It is obvious that the procedure is polynomial-time.

### A.2 3SAT v.s. HCP

#### A.2.1 REDUCTION FROM 3SAT TO HCP

Suppose we have a 3SAT instance of  $N_v$  variables  $\{x_0, x_1, \dots, x_{N_v-1}\}$  and  $N_c$  clauses, reducing it to an HCP instance follows the below two steps. More details of illustrations and proofs for claims in this subsection can be found in references, Section 28.12 of OpenDSA (Fouh et al., 2014) (slightly different).

**Step 1. Construct variable-clause nodes and edges.** We first construct  $2N_c$  nodes for each variable,  $2N_v N_c$  nodes in all. We call these nodes ‘‘variable-clause nodes’’. We assign the indices 0 to  $2N_v N_c - 1$  to these nodes. For a variable  $x_i$ , the indices of corresponding nodes are from  $2N_c i$  to  $2N_c(i+1) - 1$ . Then we construct edges  $(m, m+1)$  and  $(m+1, m)$  for  $m$  ranges from  $2N_c i$  to  $2N_c(i+1) - 2$ . If  $i < N_v - 1$ , we further construct four edges  $(2N_c i, 2N_c(i+1))$ ,  $(2N_c i, 2N_c(i+2) - 1)$ ,  $(2N_c(i+1) - 1, 2N_c(i+1))$ , and  $(2N_c(i+1) - 1, 2N_c(i+2) - 1)$ ; else if  $i = N_v - 1$ , we construct four edges  $(2N_c i, 0)$ ,  $(2N_c i, 2N_c - 1)$ ,  $(2N_c(i+1) - 1, 0)$ , and  $(2N_c(i+1) - 1, 2N_c - 1)$ .

**Step 2. Construct clause nodes and edges.** We then construct  $N_c$  nodes for the clauses. We call these nodes ‘‘clause nodes’’. We denote the clauses as  $\{C_1, C_2, \dots, C_{N_c-1}\}$ . We assign indices from  $2N_v N_c$  to  $2N_v N_c + N_c - 1$ . If clause  $C_j$  contains variable  $x_i$ , then we construct edges  $(2N_c i + 2j, 2N_v N_c + j)$  and  $(2N_v N_c + j, 2N_c i + 2j + 1)$ . If clause  $C_j$  contains variable  $\neg x_i$ , then we construct edges in the opposite directions, i.e.,  $(2N_v N_c + j, 2N_c i + 2j)$  and  $(2N_c i + 2j + 1, 2N_v N_c + j)$ .

So far, we have reduced the 3SAT instance to the graph of a HCP instance  $G$  containing  $2N_v N_c + N_c$  nodes in polynomial time. It can be easily proved that the 3SAT is satisfiable if and only if  $G$  has a Hamiltonian path.

## 972 A.2.2 TRANSFORM HCP SOLUTION TO 3SAT SOLUTION

973  
974 If the tour  $\tau$  traverse two variable-clause nodes whose index are  $2N_c i + 2j$  and  $2N_c i + 2j + 1$  in the  
975 order  $2N_c i + 2j \rightarrow$  a clause node  $\rightarrow 2N_c i + 2j + 1$ , then the variable  $x_i$  is set to True; else if the  
976 order is  $2N_c i + 2j + 1 \rightarrow$  a clause node  $\rightarrow 2N_c i + 2j$ , then  $x_i$  is set to False.

## 978 B ADDITIONAL RELATED WORK

979  
980 Apart from the literature mentioned in the main context, we hereby present a detailed summary of  
981 related works including conventional methods for TSP solving, machine learning methods for TSP  
982 solving, recent pursuit for a unified framework towards general combinatorial optimization, and  
983 specific solvers for HCP and SAT problem.

### 985 B.1 CONVENTIONAL SOLVERS

986  
987 **Exact Solvers.** Solvers for linear programming and mixed integer linear programming, including  
988 Gurobi (Gurobi Optimization, 2021) and CPLEX (Studio, 2020), can be used to solve general  
989 TSP with optimal solutions as output. Concorde is a famous TSP solver but is only applicable  
990 to 2D symmetric TSP (Hahsler & Hornik, 2007), and according to our preliminary trials, few  
991 open-source implementations produce stable and efficient solutions to ATSP. These methods can be  
992 time-consuming, especially in real-world applications where the scale of instances may be large.

993  
994 **Heuristic Solvers.** Heuristic algorithms include nearest neighbor (NN), furthest insertion (FI), etc.  
995 Among the heuristics, LKH (currently LKH-3.0.9 (Helsgaun, 2017)) is the most famous one for its  
996 high efficiency and near-optimal solutions. Technical details of LKH has been elaborated in the main  
997 context.

### 998 B.2 LEARNING METHODS FOR TSP

999  
1000 The learning models for TSP solving generally receive input features from the instance graph, where  
1001 typically the node features indicates the 2D coordinates of the nodes, and edge features indicating  
1002 the weight of the edges. These neural methods can be generally categorized into two classes, i.e.,  
1003 autoregressive (AR) and non-autoregressive (NAR) methods, according to their learning and inference  
1004 paradigm.

1005  
1006 **NAR Methods.** Non-autoregressive models usually output neural heatmaps in a one-shot manner,  
1007 indicative of the predicted likelihood of each edge being included in the optimal solution. These  
1008 networks are mostly developed on the basis of GNN or its variants. GCN (Joshi et al., 2019), Att-  
1009 GCN (Fu et al., 2021) are representative works that adopts graph convolutional network (Kipf &  
1010 Welling, 2016) for edge prediction using supervised solution proximity. UTSP (Min et al., 2024)  
1011 proposes a unsupervised framework based on Scattering Attention GNN (SAG) (Min et al., 2021).  
1012 DIMES (Qiu et al., 2022) devises a novel meta-reinforce learning framework to work cooperatively  
1013 with the active search technique for scaled 2D-TSP instances. The physics-inspired GNN (Schuetz  
1014 et al., 2022) presents to leverage the Quadratic Unconstrained Binary Optimization (QUBO) and  
1015 Ising models from statistical physics to encode optimization problems as differentiable loss functions  
1016 to support scalable unsupervised learning, but the design of Hamiltonian formulation of specific  
1017 problem can be difficult. Authors of Xia et al. (2024) also demonstrate the limitations of heatmap  
1018 generation for TSP. Deviating from the prediction of a single solution with supervised learning,  
1019 generative modeling methods (Sun & Yang, 2023; Li et al., 2023; Hottung et al., 2021a) endeavor to  
1020 characterize a distribution of high-quality solutions for a given instance. Solutions can be established  
1021 by sampling from the distribution. GNARKD (Xiao et al., 2024) obtains NAR VRP solvers through  
1022 knowledge distillation, but limited its evaluation to symmetric TSP and CVRP.

1023  
1024 **AR Methods.** Instead of global prediction in one shot, sequence models decompose the TSP task  
1025 into an n-step node prediction, where each step offers the prediction map of the next node selection  
based on the current state. The sequence models generally follow an attention based encoder-decoder  
model where the encoder produces embeddings of all input nodes and the decoder produces the  
per-step node predictions accordingly. RL4CO community develops a comprehensive repository for

1026 this category of methods (Berto et al., 2024). Representatively, AM (Kool et al., 2018) first proposes  
 1027 using transformer-based attention model for routing problems. POMO (Kwon et al., 2020) proposes  
 1028 the policy optimization with multiple optima for reinforcement learning; Sym-NCO (Kim et al., 2022)  
 1029 leverages symmetry for neural combinatorial optimization, which is widely adopted in subsequent  
 1030 literature. Recent work BQ-NCO (Drakulic et al., 2023) introduces a novel Markov Decision Process  
 1031 (MDP) formulation for COPs, leveraging bisimulation quotienting to enhance out-of-distribution  
 1032 robustness.

1033  
 1034 **Divide-and-Conquer Frameworks** In the context of neural solvers for combinatorial optimization,  
 1035 scalability has been a longstanding concern and challenge for the community. For NAR methods, we  
 1036 notice that acquiring supervision for edge regret is extremely time-consuming, making it impractical  
 1037 for solving larger-scale problems than TSP-500. Meanwhile, RL-based sequence models also face  
 1038 challenges on larger-scale problems due to issues like sparse rewards and training instability, which  
 1039 also struggle to support training on larger-scale instances (even impractical for  $N \geq 100$ ). To  
 1040 address this issue, apart from effort to tailor specific architectures or training techniques, resorting to  
 1041 divide-and-conquer is proven feasible and performant. Authors of Fu et al. (2021) train a small-scale  
 1042 model, which could be repetitively used to build heat maps for TSP instances of arbitrarily large size.  
 1043 Luo et al. (2024) proposes a novel Self-Improved Learning method for better scalability of neural  
 1044 combinatorial optimization, powered by an innovative local reconstruction approach that iteratively  
 1045 generates better solutions by itself as pseudo-labels to guide efficient model training. Most recently,  
 1046 GLOP (Ye et al., 2024b) learns to partition large routing problems into TSPs and TSPs into Shortest  
 1047 Hamiltonian Path Problems (SHPPs), which subsequently get conquered by local revisers. These  
 methods improve the scales of TSPs applicable to neural solvers up to 10000 nodes.

1048 **Remarks.** It should be highlighted that the effective divide-and-conquer frameworks are indeed  
 1049 orthogonal to our proposed generic solver, where a significant synergy can be reached to enhance  
 1050 both model scalability and solving quality.

### 1051 1052 B.3 COMBINATION OF NEURAL AND OR METHODS

1053  
 1054 In addition to end-to-end approaches for CO problems on graphs (COPG), resorting to the com-  
 1055 bination of neural networks and operations research (OR) methods is studied in several works.  
 1056 VSRLKH (Zheng et al., 2021) and NeuroLKH (Xin et al., 2021) combines the strong traditional  
 1057 heuristic Lin-Kernighan-Helsgaun (LKH) for TSP with reinforcement learning and supervised learn-  
 1058 ing respectively. GNNGLS (Hudson et al., 2021) and NeuralGLS (Sui et al., 2023) present hybrid  
 1059 approaches for solving the TSP based on GNNs and Guided Local Search (GLS), which searches  
 1060 for solutions from neurally predicted regret of including each edge. da Costa et al. (2020), Sui  
 1061 et al. (2021) and Ma et al. (2023) are similar works that solve TSP through automatically learning  
 1062 effective 2-, 3- and k-opt heuristics in a data-driven manner. DPDP (Kool et al., 2022) proposes a  
 1063 Deep Policy Dynamic Programming (DPDP) scheme, which aims to combine the strengths of learned  
 1064 neural heuristics with those of DP algorithms. However, it only scales up to 100 nodes in terms of  
 1065 solving TSPs and VRPs. DeepACO (Ye et al., 2024a) is a meta-heuristic algorithm which leverages  
 1066 deep reinforcement learning to automate heuristic designs. GFACS (Kim et al., 2024) develops a  
 neural-guided probabilistic search algorithm for solving COPs.

1067 **Remarks.** A common limitation of these methods is the over dependence of their performance on  
 1068 the effectiveness of the local search, rendering the necessity of the neural parts questionable.

### 1069 1070 B.4 MULTI-TASK CO MODELS

1071  
 1072 Recent literature show growing interest of general neural CO solver for multiple problems. While  
 1073 similar concepts, e.g., “multi-task solver”, “universal solver”, etc., have frequently appeared in some  
 1074 latest works, they often denote quite different approaches and functionalities. For example, MTCO  
 1075 (Li & Liu, 2023) devises a “multi-task” CO framework which first measures the similarity between  
 1076 CO problems, and then transfers knowledge between similar instances within the *same* problem  
 1077 type to gain search speed-ups in its quadratic programming solver. However, it primarily focuses  
 1078 on the permutation flowshop scheduling problem (PFSP) and does not explore the application of its  
 1079 method in handling different types of problems. Moreover, MTCO is not specifically designed for  
 learning-based neural solvers, making the term “multi-task” in its title misleading from a learning

Table 6: Comparison of different recent works that involve “multi-task” or “general TSP” solving. “Multi-Task”: Whether the method aims for multi-task CO solving. “Multi-Scale”: Whether the model adapts to differently scaled instances on the fly without pre-setting parameters. “Single Solver”: Whether a unified solver learns multiple problems simultaneously. “General TSP”: Whether the method supports general TSP input, i.e., (probably asymmetric or discrete) distance matrix only. “QP”: Quadratic Programming. “RL”: Reinforcement Learning. “SL”: Supervised Learning. “Evaluated Scale”: the first line means the maximal (TSP/VRP) scale in the main experiments, and the second line (if exists) means the maximal scale evaluated in additional experiments (supplementary results, divide-and-conquer application, generalizability, etc.). “✓\*”: limited to variants of VRPs.

Method	Evaluated Problems	Applicable Problems	Evaluated Scale	Multi-Task	Multi-Scale	Single Solver	General TSP	Solver Type
MTCO (Li & Liu, 2023)	PFSP		N/A	✗	✓	✗	✗	QP
ASP (Wang et al., 2024)	TSP, CVRP	N/A	100 (~300)	N/A	N/A	N/A	✗	ML-based
MAB-MTL (Wang & Yu, 2023)	TSP, CVRP, OP, KP		100	✓	✓	✗	✗	RL
MVMoE (Zhou et al., 2024)	16 VRPs	VRP variants	100 (1000)	✓*	✓	✓	✗	RL
MTNCO (Liu et al., 2024)	11 VRPs	VRP variants	100 (~1000)	✓*	✓	✓	✗	RL
UNCO (Jiang et al., 2024)	TSP, CVRP, KP, MVCP, SMTWTP		100	✓	✓	✓	✗	LLM + RL
GOAL (Drakulic et al., 2024)	ATSP, CVRP, OP, JSSP		100 (1000)	✓	✓	✓	✓	SL
MatNet (Kwon et al., 2021)	ATSP, FFSP	$\mathcal{P}$ in matrix format	100	✗	✗	✗	✓	RL
DIMES (Qiu et al., 2022)	TSP, MIS		10K	✗	✗	✗	✗	Meta-RL
BQ-NCO (Drakulic et al., 2023)	TSP, ATSP, CVRP, OP		100 (1000)	✗	✗	✗	✓	RL
GLOP (Ye et al., 2024b)	TSP, ATSP, CVRP, PCTSP	(Large) VRPs	10K (100K)	✗	✓	✗	✓	RL
RedCO (Ours)	ATSP, TSP, HCP, SAT	$\mathcal{P} \leq_P$ general TSP or $\mathcal{P}$ in matrix format (VC, Clique, VRPs, FFSP, MIS, etc.)	100 (10K)	✓	✓	✓	✓	RL, Meta-RL, SL, Generative, etc.

perspective and irrelevant to the theme of this paper. ASP (Wang et al., 2024) proposes a “universal” framework to address generalization issues of neural CO solvers, which iteratively improves the generalizability to different distributions (including scales). ASP proposes a model-/problem-agnostic training policy to improve generalizability. However, it is also focused on PFSP, and does not provide a specific neural solver which we believe is technically nontrivial that can deal with different types of problems. In the work (Wang & Yu, 2023), authors propose a multi-armed bandit framework to train a neural solver for different CO problems, whereby problems share a common encoder but differ in the header and the decoder. Yet, as the header and decoder necessitate customized designs for specific problems, the solver cannot be readily applied to unseen problems, restricting its applicability to the training dataset comprising TSP, CVRP, OP and KP. MVMoE (Zhou et al., 2024) develops a multi-task VRP solver with mixture-of-experts utilizing a hierarchical gating mechanism, which achieves good zero-shot generalization performance on multiple VRP variants. Boisivert et al. (2024) proposes a new generic representation that encodes problem constraints into a graph structure by breaking down each constraint into an abstract syntax tree and connecting related variables and constraints through edges. However, the authors also identify limitations in terms of training time and the size of the generated graphs. Resembling MVMoE, MTNCO (Liu et al., 2024) tackles the cross-problem generalization among variants of VRPs using shared underlying attributes and solve them simultaneously via a single model through attribute composition. More recently, UNCO (Jiang et al., 2024) resorts to large language models (LLMs) that take natural language to formulate text-attributed instances for different COPs and encode them in the same embedding space, thereby facilitating a unified process of solution construction. But the solving quality and scalability has considerable room for improvement. GOAL (Drakulic et al., 2024) proposes a single backbone plus light-weight problem specific adapters that solves a variety of COPs include ATSP but with inferior performance.

## B.5 SPECIFIC SOLVERS FOR SAT AND HCP

**SAT.** Neural methods for solving the SAT problem can be broadly classified into two categories: standalone neural solvers and neural-guided solvers. Direct neural solvers, such as NeuroSAT (Selsam et al., 2018) and subsequent works (Cameron et al., 2020; Jaszczur et al., 2020), classify CNF formulas as satisfiable or unsatisfiable while simultaneously constructing possible assignments by decoding literal embeddings. Several alternative approaches (Amizadeh et al., 2018; 2019; Ozolins et al., 2022) focus on directly generating satisfying assignments, leveraging different GNN architectures and employing unsupervised loss for training. These methods generally aim to predict a single satisfying solution for each instance, failing to account for other possible solutions. In the category of neural-guided methods, NeuroCore (Selsam & Björner, 2019) and #Neuro (Vaezipoor et al., 2021) utilize neural networks to guide the branching decisions of SAT and #SAT solvers. NSNet (Li & Si, 2022) models satisfiability problems as probabilistic inference, using a graph neural network (GNN) to parameterize belief propagation (BP) in the latent space, thereby guiding a local search for a satisfying assignment. Readers can refer to Guo et al. (2023) for a thorough survey of solving SAT problem with neural approaches.

**HCP.** It is noteworthy that HCP have not yet been extensively discussed within the ML4CO community. One recent work incorporating HCP as a case study is Wang et al. (2021), which proposes a bi-level framework with an upper-level learning method to optimize the graph (e.g., adding, deleting, or modifying edges), combined with a lower-level heuristic algorithm solving the optimized graph. This framework utilizes an actor-critic-based RL method to train a graph convolutional network (GCN) and tests it on 1001 large HCP instances, achieving results comparable to LKH.

## B.6 NOTE ON EVALUATION OF SPECIFIC SOLVERS

It can be controversial that we have not yet incorporated the so-called “specialized solvers” for the individual type of CO problems covered in this paper. We hereby provide our detailed consideration and clarification upon this issue in hope to eliminate possible ambiguity and misunderstanding.

**Conforming to Our Motivation.** As our primary motivation goes, proposing a competitive yet compact workflow capable of effectively tackling (A)TSP instances with different problem distributions comes foremost.

**Lack of Companion Methods.** To our best knowledge, few existing specialized solvers match our formulation of CO problems, nor are there prevalent evaluation protocols. Notably, there is limited exploration of the potential to unify various combinatorial optimization problems on graphs and exploit matrix representations for developing neural solvers with cross-task universality or cross-distribution robustness.

**Existing Research Convention.** There is precedent in top literature for evaluating different problems within a primarily targeted problem type. E.g., in NeuroSAT (Selsam et al., 2018), the authors, despite focusing on a new SAT solver, gained recognition for its cross-task applicability by modeling and solving graph coloring, dominating-set, and node cover problems within the SAT formulation.

**Remarks.** Therefore, it is supposed to be reasonable to compare within the scope of general TSP solvers on our unified matrix datasets where various CO tasks are implicitly embedded, also in hope to facilitate standardized comparison of the general neural combinatorial optimization community.

## C NETWORK DETAILS

### C.1 VANILLA MATNET AND MATPOENET

**Encoder.** Each node  $i$  in the graph form of the input matrix is assigned with two embedding vectors<sup>2</sup>  $\mathbf{a}_i, \mathbf{b}_i \in \mathbb{R}^d$ . We denote the embedding matrix of all nodes at the  $l$ -th layer as  $\mathbf{A}^l = [\mathbf{a}_1^l, \mathbf{a}_2^l, \dots, \mathbf{a}_N^l] \in \mathbb{R}^{d \times N}$  and  $\mathbf{B}^l$  of the same shape. The input  $\mathbf{A}^0$  and  $\mathbf{B}^0$  are initialized as zero embeddings and one-hot embeddings respectively. Note that  $\mathbf{B}^0$  may not be a square matrix, so MatNet forces  $d \geq N$  and set  $\mathbf{B}^0$  as an one-hot square matrix  $\mathbf{OE} \in \mathbb{R}^{N \times N}$  padded with zero values

<sup>2</sup>By default, all mentioned vectors are column vectors.

$\mathbf{0} \in \mathbb{R}^{N \times (d-N)}$ , i.e., mathematically  $\mathbf{B}^0 = [\mathbf{OE}, \mathbf{0}]^\top$ . Notably,  $\mathbf{B}^0 = \mathbf{POE}$  in MatNetPOE and need not paddings.

Taking embedding  $\mathbf{A}$  as example:

$$\mathbf{Q}_a^l = \mathbf{W}_a^Q \mathbf{A}^l, \mathbf{K}_a^l = \mathbf{W}_a^K \mathbf{B}^l, \mathbf{V}_a^l = \mathbf{W}_a^V \mathbf{B}^l, \quad (10)$$

$$\text{MixedScoreAtt}_a^l = \text{softmax}\left(\text{MLP}_1\left([\mathbf{C}; \frac{\mathbf{Q}_a^{l\top} \mathbf{K}_a^l}{\sqrt{d_{qkv}}}\right]\right), \quad (11)$$

$$\mathbf{A}^{l+1} = \text{MLP}_2\left(\text{MixedScoreAtt}_a^l \mathbf{V}_a^{l\top}\right)^\top, \quad (12)$$

where  $\mathbf{W}_a^Q, \mathbf{W}_a^K, \mathbf{W}_a^V \in \mathbb{R}^{d_{qkv} \times d}$  are learnable parameters for attention modeling.  $[\cdot; \cdot]$  denotes the concatenation operation,  $\text{MLP}(\cdot)$  denotes a multilayer perceptron layer with activation functions and batch normalization operations inside. The input and output dimensions of  $\text{MLP}_1$  are 2 and 1 respectively, so  $\text{MLP}_1$  achieves to mix the attention values and the cost matrix, yielding the mixed score  $\text{MixedScoreAtt}_a^l \in \mathbb{R}^{N \times N}$ . The input and output dimensions of  $\text{MLP}_2$  is are both  $d$ .

Computing  $\mathbf{B}^{l+1}$  is completely symmetrical with  $\mathbf{A}^{l+1}$  as shown in Eq. 10 to Eq. 12, by exchanging the positions of  $\mathbf{A}^l$  and  $\mathbf{B}^l$  and introducing new parameters  $\mathbf{W}_b^Q, \mathbf{W}_b^K, \mathbf{W}_b^V$ .

MatNet extends the mixed-score attention to a multi-head one, just as the original Transformer (Vaswani et al., 2017).

**Decoder.** Given the output embedding  $\mathbf{A}$  and  $\mathbf{B}$  of the last layer of the encoder, the decoder aims to conduct the so-called ‘rollout’ to obtain a tour  $\tau = \{i_1, i_2, \dots, i_N\}$ . The first step is to compute the key and value matrices by  $\mathbf{K}_{dec} = \mathbf{W}_{dec}^K \mathbf{B}$  and  $\mathbf{V}_{dec} = \mathbf{W}_{dec}^V \mathbf{B}$ , where  $\mathbf{W}_{dec}^K, \mathbf{W}_{dec}^V \in \mathbb{R}^{d_{qkv} \times d}$  are trainable parameters. When node  $i_n$  is selected as  $n$ -th node in the tour  $\tau$ , the query vector  $\mathbf{q}_{dec}^{n+1} \in \mathbb{R}^{d_{qkv}}$  containing information of previously selected nodes  $\{i_1, \dots, i_n\}$  is computed by:

$$\mathbf{q}_{dec}^1 = \mathbf{W}_{dec}^{Q^1} \mathbf{a}_{i_1}, \mathbf{q}_{dec}^{n+1} = \mathbf{W}_{dec}^{Q^0} \mathbf{a}_{i_n} + \mathbf{q}_{dec}^1, \quad (13)$$

where  $\mathbf{W}_{dec}^{Q^1}, \mathbf{W}_{dec}^{Q^0} \in \mathbb{R}^{d_{qkv} \times d}$  are trainable parameters for the query vectors. Then, the output embedding of  $n$ -th iteration of the rollout  $\mathbf{o}_{dec}^{n+1}$  can be obtained by:

$$\mathbf{o}_{dec}^{n+1} = \text{Linear}\left(\text{softmax}\left(\text{Inf}_{i_{n' \leq n}} + \frac{\mathbf{q}_{dec}^{n\top} \mathbf{K}_{dec}}{\sqrt{d_{qkv}}}\right) \mathbf{V}_{dec}\right), \quad (14)$$

where  $\text{Inf}_{i_{n' \leq n}}$  is a vector of length  $N$  whose  $i_{n'}$ -th element is set to negative infinity for all  $n' \leq n$  and other elements are set to 0,  $\text{Linear}(\cdot)$  is a linear layer whose input dimension is  $d_{qkv}$  and output dimension is  $d$ . In practice, Eq. 14 is further enhanced by multi-head attention. By Eq. 14,  $\mathbf{o}_{dec}^{n+1}$  becomes a linear combination of the embeddings  $\mathbf{b}_s$  of unselected nodes, while the weights are determined by the selected nodes whose information is contain in  $\mathbf{q}_{dec}^n$ .

The probability vector to select the next node  $i_{n+1}$  is:

$$\mathbf{p}_\theta(i_{n+1} | i_{n' \leq n}) = \text{softmax}\left(\text{Inf}_{i_{n' \leq n}} + \tanh\left(\frac{\mathbf{B}^\top \mathbf{o}_{dec}^{n+1}}{\sqrt{d}}\right)\right). \quad (15)$$

After  $N$  rollout iterations, a complete tour can be obtained.

**Model training.** It is trained in the same way as POMO (Kwon et al., 2020) based on DRL. For each instance with  $\mathbf{C}$ , it samples  $N$  tours  $\{\tau^1, \tau^2, \dots, \tau^N\}$  with different nodes as start. Then the policy gradient is:

$$\nabla_\theta J(\theta) \approx \frac{1}{N} \sum_{n=1}^N (L(\tau^n) - b(\mathbf{C})) \nabla_\theta \log p_\theta(\tau^n | \mathbf{C}), \quad (16)$$

where  $L(\tau)$  is the length of tour  $\tau$ ,  $b(\mathbf{C})$  is a baseline method which is instantiated as the mean tour length of the  $N$  tours, mathematically  $b(\mathbf{C}) = 1/N \sum_{n=1}^N L(\tau^n)$ .

Fig. 4 illustrates the general neural structure of MatPOENet, highlighting with dashed square the adaptive design for initial node embedding, i.e., the scale-free initializer, pseudo one-hot embedding scheme.

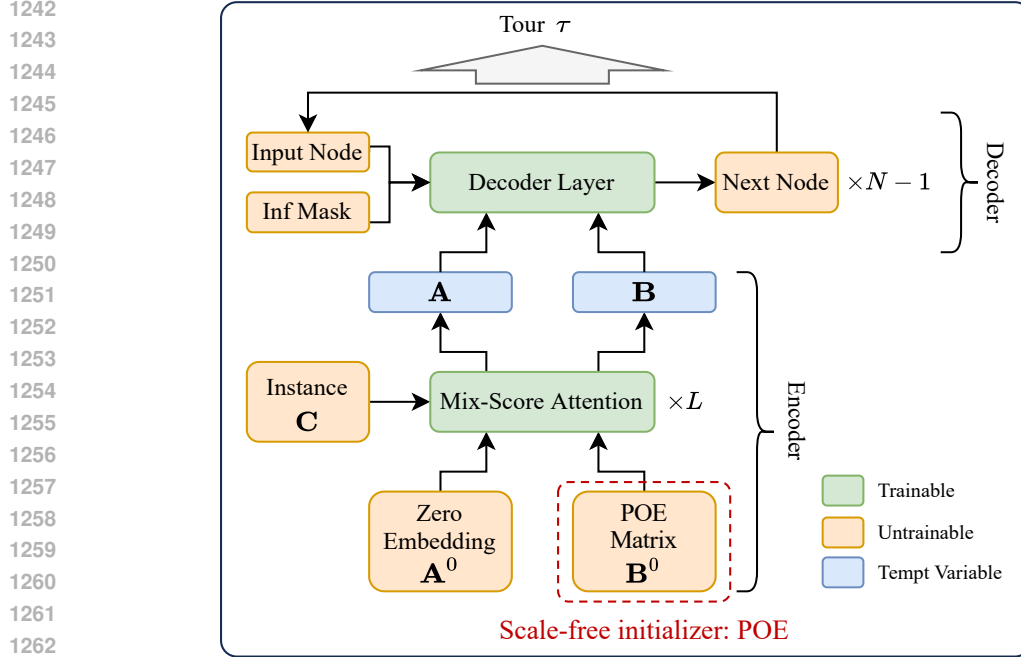


Figure 4: General structure of MatPOENet.

## C.2 GRAPH-BASED DIFFUSION AND MATDIFFNET

**Overview.** Given the distribution of problem instance with distance matrix  $C$ , solutions ( $S$ ) can be established by sampling from the distribution and maximizing the conditional likelihood estimation  $\mathbb{E}[\log p_\theta(S|C)]$ , where  $\theta$  is the model parameters. The model is optimized through the evidence lower bound (ELBO) in Eq. 17, where  $q$  is the posterior and  $Z$  is the latent variable.

$$\mathcal{L} = -\mathbb{E}_q(z|S, C) \left[ \log \frac{p_\theta(S, Z|C)}{q(Z|S, C)} \right] \geq \mathbb{E}[-\log p_\theta(S|C)]. \quad (17)$$

**Details.** MatDIFFNet generates general TSP solutions  $S_0 \in \{0, 1\}^{n \times n}$  by  $T$ -step denoising process from random noises  $S_T$ , and the latent variables include noised solution  $S_{1:T}$ , outputting a binary heatmap guiding the search of a valid TSP tour. The discrete diffusion models generate solutions  $S_0 \in \{0, 1\}^{n \times n}$  by  $T$ -step denoising process from random noises  $S_T$ , and the latent variables include noised solution  $S_{1:T}$ . For each entry, the model estimates a Bernoulli distribution indicating whether this entry should be selected. In implementation, each entry of solution is represented by a one-hot vector<sup>3</sup> such that  $S_0 \in \{0, 1\}^{n \times n \times 2}$ . Following the notations of Ho et al. (2020); Austin et al. (2023), the general framework of diffusion includes a forward noising and a reverse denoising Markov process. The noising process takes the initial solution  $S_0$  and progressively introduces noise to generate a sequence of latent variables  $S_{1:T}$ . The denoising process is learned by the model, which starts from the final latent variable  $S_T$  and denoises  $S_t$  at each time step to generate the preceding variables  $S_{t-1}$  based on the instance  $C$ , eventually recovering the target data distribution. The formulation of the denoising process is expressed as  $p_\theta(S_{0:T}|C) = p(S_T) \prod_{t=1}^T p_\theta(S_{t-1}|S_t, C)$ . The training optimization aims to align  $p_\theta(S_0|C)$  with the data distribution  $q(S_0|C)$  using ELBO:

$$\mathcal{L} = \mathbb{E}_q \left[ \sum_{t>1} D_{KL} [q(S_{t-1}|S_t, S_0) \| p_\theta(S_{t-1}|S_t, C)] - \log p_\theta(S_0|S_1, C) \right] + C. \quad (18)$$

Specifically, the forward noising process is achieved by multiplying  $S_t \in [0, 1]^{N \times N \times 2}$  at step  $t$  with a forward transition probability matrix  $Q_t \in [0, 1]^{2 \times 2}$  where  $[Q_t]_{i,j}$  indicates the probability of transforming  $E_i$  in each entry to  $E_j$ . We set  $Q_t = \begin{bmatrix} \beta_t & 1 - \beta_t \\ 1 - \beta_t & \beta_t \end{bmatrix}$  (Austin et al., 2023),

<sup>3</sup>Each entry with  $[0, 1]$  indicates that it is included in  $S$  and  $[1, 0]$  indicates the opposite.



where  $\beta_t \in [0, 1]$  such that the transition matrix is doubly stochastic with strictly positive entries, ensuring that the stationary distribution is uniform which is an unbiased prior for sampling. The noising process for each step and the  $t$ -step marginal are formulated as:

$$q(\mathbf{S}_t|\mathbf{S}_{t-1}) = \text{Cat}(\mathbf{S}_t; \mathbf{p} = \mathbf{S}_{t-1}\mathbf{Q}_t) \quad \text{and} \quad q(\mathbf{S}_t|\mathbf{S}_0) = \text{Cat}(\mathbf{S}_t; \mathbf{p} = \mathbf{S}_0\bar{\mathbf{Q}}_t), \quad (19)$$

where  $\text{Cat}(\mathbf{S}; \mathbf{p})$  is a categorical distribution over  $N$  one-hot variables with probabilities given by vector  $\mathbf{p}$  and  $\bar{\mathbf{Q}}_t = \mathbf{Q}_1\mathbf{Q}_2 \cdots \mathbf{Q}_t$ . Through Bayes' theorem, the posterior can be achieved as:

$$q(\mathbf{S}_{t-1}|\mathbf{S}_t, \mathbf{S}_0) = \frac{q(\mathbf{S}_t|\mathbf{S}_{t-1}, \mathbf{S}_0)q(\mathbf{S}_{t-1}|\mathbf{S}_0)}{q(\mathbf{S}_t|\mathbf{S}_0)} = \text{Cat}\left(\mathbf{S}_{t-1}; \mathbf{p} = \frac{\mathbf{S}_t\mathbf{Q}_t^\top \odot \mathbf{S}_0\bar{\mathbf{Q}}_{t-1}}{\mathbf{S}_0\bar{\mathbf{Q}}_t\mathbf{S}_t^\top}\right). \quad (20)$$

The neural network is trained to predict the logits of the distribution  $\tilde{p}_\theta(\tilde{\mathbf{S}}_0|\mathbf{S}_t, \mathbf{C})$ , such that the denoising process can be parameterized through  $q(\mathbf{S}_{t-1}|\mathbf{S}_t, \tilde{\mathbf{S}}_0)$ :

$$p_\theta(\mathbf{S}_{t-1}|\mathbf{S}_t) \propto \sum_{\tilde{\mathbf{S}}_0} q(\mathbf{S}_{t-1}|\mathbf{S}_t, \tilde{\mathbf{S}}_0)\tilde{p}_\theta(\tilde{\mathbf{S}}_0|\mathbf{S}_t, \mathbf{C}). \quad (21)$$

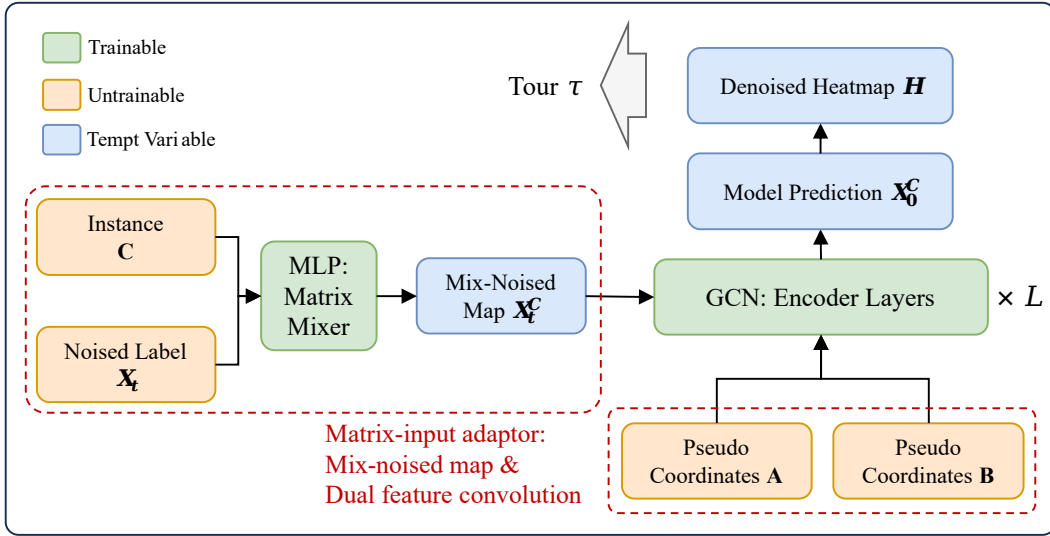


Figure 5: General structure of MatDIFFNet.

Fig. 5 illustrates the general neural structure of MatDIFFNet, highlighting with dashed square the adaptive design for matrix input, i.e., the mix-noised reference map and dual feature convolution scheme.

## D EXPERIMENTAL DETAILS

### D.1 HYPERPARAMETERS

**MatPOENet.** We set 512 as the positional embedding dimension as well as all hidden dimensions in the network. For  $N \approx 20$  and 50, 8 layers of mix-score attention block is adopted to better capture problem features, whereas 5 layers are set for  $N \approx 100$  for space saving. We train our model using Adam optimizer (Kingma, 2014) with a learning rate of  $4 \times 10^{-4}$  with a decay of  $1 \times 10^{-6}$ . The batch size is set to 200 for  $N \approx 20, 50$  and 150 for  $N \approx 100$ . Defining a training epoch as 10,000 randomly generated problem instances, we find the performance sufficiently noteworthy within 2,000 epochs for all scales, despite the fact that more training steps might produce better convergence and outcomes.

**MatDIFFNet.** The parameter setting of MatDIFFNet basically follows Li et al. (2023). We set the dimension of the input features for implemented graph neural networks equals 2 indicating the pseudo 2D coordinates of the nodes, and set the feature dimension of the intermediate layers to 256. The output channel dimensions of the networks are set as 2 for the classification modelling. Default number of GNN layers is set to 12. Models at all scales are trained with a cosine learning rate schedule starting from  $4 \times 10^{-4}$  and ending at 0. For each type of problem distribution, we generally use 1.28M random instances for each epoch of training and train the models for 100 epochs. We apply curriculum learning and initialize the models from  $N \approx 50$  checkpoints. For mixed data training, 400 epochs are conducted to gain an equivalent period to those trained individually. Training batch-size is set to 128 for  $N \approx 50$  and 32 for  $N \approx 100$ . For the diffusion part, We implement the model with 50 inference steps for denoising, and the models are trained with 1000 denoising steps, i.e.,  $T_{denoise} = 1000$ . We additionally apply the technique of denoising diffusion implicit models (DDIMs (Song et al., 2020)) for accelerating inference and solution reconstruction.

**RedCO-DIMES.** We set 8 layers for the backbone GNN with 64 hidden units for each. For both outer updates and inner meta-steps, we use AdamW (Loshchilov & Hutter, 2018) as optimizer, with a learning rate of  $1 \times 10^{-3}$  and  $1 \times 10^{-1}$  respectively. For all scales of problems, we train the model for 1000 outer epochs, each containing  $T_{meta} = 15$  inner meta-updates with  $K = 1000$  samples. In the testing phase, we set the (inner) learning rate of active search to 0.5 for faster optimization and with a typical 100 steps.

## D.2 SCALE SETTING OF 3SAT INSTANCES

To align with our experimental setup ( $N \approx 20, 50, 100$ ), we manually tailor the number of variables  $N_v$  and clauses  $N_c$  as outlined in Table 7. During training at a specific scale, each batch of 3SAT instances are generated with a randomly determined parameter line within the corresponding scale group.

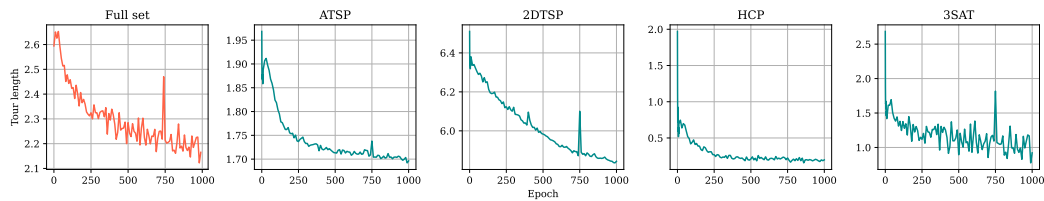
Table 7: Detailed scale parameters of 3SAT instances contained in different experimental groups.

Scale group	# Variables ( $N_v$ )	# Clauses ( $N_c$ )	Exact $N$	Average $\bar{N}$
$N \approx 20$	4	2	18	20.3
	3	3	21	
	5	2	22	
$N \approx 50$	6	3	39	49.8
	3	7	49	
	6	4	52	
	4	6	54	
	5	5	55	
$N \approx 100$	9	5	95	101.0
	5	9	99	
	8	6	102	
	6	8	104	
	7	7	105	

## D.3 TRAINING CURVES

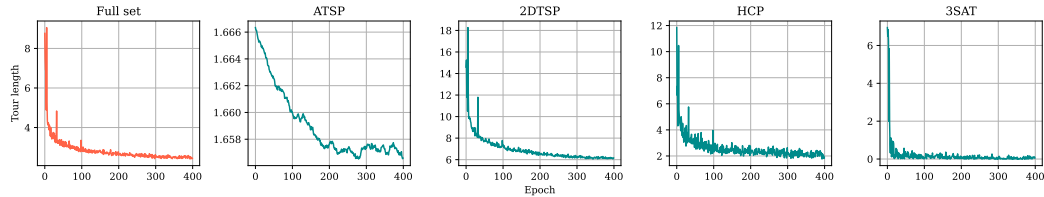
Fig. 6, Fig. 7, and Fig. 8 depict the solved tour length during the training process of MatPOENet, MatDIFFNet, and DIMES under our RedCO framework. Note that the ATSP curve for MatDIFFNet is smoothed by exponential moving average with  $\alpha = 0.01$  for better clarity, as it reaches the fluctuation stage sharply within the initial epochs. The RL-based training curves (MatPOENet and DIMES) are sampled with a time step of 10. It can be observed that Transformer-, Diffusion- and GNN-based backbones are all well optimized under RedCO with problem instance reduction. Furthermore, detailed training objective curves for each individual problem type demonstrate consistency and stability of convergence across all involved problem categories, addressing our claim of multi-task robustness.

1404  
1405  
1406  
1407  
1408  
1409  
1410  
1411



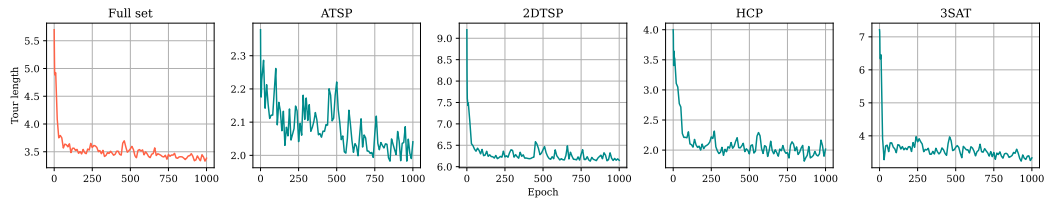
1412 Figure 6: Tour length of different problem categories during RedCO-empowered mixed-data training  
1413 of MatPOENet with  $N \approx 50$ .

1414  
1415  
1416  
1417  
1418  
1419  
1420  
1421



1422 Figure 7: Tour length of different problem categories during RedCO-empowered mixed-data training  
1423 of MatDIFFNet with  $N \approx 50$ .

1424  
1425  
1426  
1427  
1428  
1429  
1430  
1431  
1432



1433 Figure 8: Tour length of different problem categories during RedCO-empowered mixed-data training  
1434 of DIMES-AS with  $N \approx 50$ .

## 1435 E MORE APPLICATIONS OF REDCO

1436  
1437  
1438  
1439  
1440  
1441  
1442  
1443  
1444  
1445

In this section, we provide the details of possible applications of our proposed RedCO. For backbone model, we adapt DIMES (Qiu et al., 2022) for multi-task training under RedCO by simply replacing its input of nodes coordinates by random vectors. In Sec. E.1, we carefully introduce its model architecture and training policy. For more applicable problems, Sec. E.2 presents a list of feasible CO problems that can **i) be reduced to general TSP form, ii) formulated via matrix representation, or iii) resolved by our proposed models as specific solvers**. In the conclusion, we provide further clarification upon the orthogonality of RedCO and the proposed backbone solvers, reiterating the motivation and position of our paper.

1446  
1447

### 1446 E.1 MORE ADAPTABLE BACKBONE: GNN-BASED DIMES

1448  
1449  
1450  
1451  
1452  
1453  
1454  
1455  
1456  
1457

DIMES (Qiu et al., 2022) proposes a scalable neural solver for 2DTSP based on meta-learning and deep RL.

For TSP, parallel to attention models that sequentially decode node selections, GNN-based techniques have gained prominence for predicting heatmaps in support of online searching. To this end, we endeavor to pinpoint a GNN-based architecture that aligns seamlessly with the implementation of our instance reduction-based general CO training framework. Several observations guide this exploration: **1) High cost of supervised training.** Preparing supervision for TSP is primarily time-consuming. Even worse, matrix input of general TSP can be intractable for space as well, compared to existing works that often take the convenience of storing coordinate representations only. **2) Embedding limitations.** Prevailing GNN methods, often designed for TSP as an edge classification task, heavily rely on coordinate inputs, which remains open problem. **3) Data distribution variability.** Notable

1458 divergence of data distribution exists subsequent to the reduction of TSP from diverse problem  
1459 instances. This variability poses a considerable challenge for supervised training of GNN.

1460 Our exploration of existing models unveil that meta-learning and RL-based active search strategies in  
1461 DIMES resonate with our intuitive perspective. We adapt vanilla DIMES into our RedCO architecture,  
1462 underscoring its proper alignment with our motivation of tackling multi-task CO problems, and in  
1463 turn validating the feasibility of our proposed framework.

1464 **Overview.** DIMES uses an Anisotropic GNN (Bresson & Laurent, 2018) as backbone to capture  
1465 representations of different types of problem instances. The vanilla DIMES takes node coordinates as  
1466 the input node features and the distances as the input edge features. To generalize DIMES to general  
1467 TSP, we empirically use random numbers sampled from  $[0, 1]$  of a fixed dimension  $d$  ( $d = 64$  by  
1468 default) as the node feature. The training process combines Model-Agnostic Meta-Learning (MAML)  
1469 and DRL. The primary objective is to enhance the prediction of heatmap initialization that later  
1470 yields optimal solving results after the RL-based active search in the testing phase. Following the  
1471 paradigm of meta-learning, the training process of DIMES involves *outer* epochs which optimizes  
1472 the backbone GNN parameters utilizing the estimated policy gradients computed with one or more  
1473 *inner* meta-updates. We present the detailed mathematical formulations below.

### 1475 E.1.1 NETWORK ARCHITECTURE

1476 The GNN layers work as the following message passing scheme:

$$1478 \mathbf{h}_i^{l+1} = \mathbf{h}_i^l + \alpha \left[ \text{BN} \left( \mathbf{U}^l \mathbf{h}_i^l + \mathcal{A}_{j \in \mathcal{N}_i} (\sigma(\mathbf{e}_{ij}^l) \odot \mathbf{V}^l \mathbf{h}_j^l) \right) \right], \quad (22)$$

$$1479 \mathbf{e}_{ij}^{l+1} = \mathbf{e}_{ij}^l + \alpha (\text{BN}(\mathbf{P}^l \mathbf{e}_{ij}^l + \mathbf{Q}^l \mathbf{h}_i^l + \mathbf{R}^l \mathbf{h}_j^l)), \quad (23)$$

1481 where  $\mathbf{h}_i^l$  and  $\mathbf{e}_{ij}^l$  respectively denote the node embedding of node  $i$  and the edge embedding of edge  
1482  $(i, j)$  at the  $l$ -th layer,  $\mathbf{U}^l, \mathbf{V}^l, \mathbf{P}^l, \mathbf{Q}^l, \mathbf{R}^l$  are learnable parameters of  $l$ -th layer,  $\alpha(\cdot)$  is the activation  
1483 function (set as SiLU (Elfwing et al., 2018) in practice),  $\text{BN}(\cdot)$  is the batch normalization function.

### 1485 E.1.2 TRAINING PROCESS

1486 Let  $F_\Phi$  denote the graph neural network parametrized by  $\Phi$ . For each TSP graph instance  $s$  reduced  
1487 from the problem pool  $C$ , the instance-specific input to the network is its distance matrix  $D_s$ , and the  
1488 output  $\theta_s \in \mathbb{R}^{n \times n} := F_\Phi(D_s)$  acts as the initial heatmap guiding the search of a TSP tour. A higher  
1489 valued  $\theta_{i,j}$  indicates a higher probability for the edge from node  $i$  to node  $j$  to be sampled. The  
1490 vanilla loss function is articulated as the expected cost of the solution for any graph in the collection:

$$1492 L(\Phi|C) = \mathbb{E}_{s \in C} S(\theta_s) = \mathbb{E}_{s \in C} S(F_\Phi(D_s)), \quad (24)$$

1494 where  $S(\cdot)$  denotes the sampling-based baseline function (Kool et al., 2019) from a given distribution  
1495 representation of predicted heatmap. Specifically, a batch of graph instances of the same problem  
1496 type and scale is generated randomly from  $C$  in every *outer* training epoch, within which  $T$  *inner*  
1497 meta-steps are taken to fine-tune the parameters on each instance by RL-based updates, referred  
1498 to as active search (Bello et al., 2016; Hottung et al., 2021b). The fine-tuned parameters  $\Phi_s^{(T)}$   
1499 are computed using these gradient updates for each graph instance  $s$  with a inner learning rate  $\alpha$ , thus  
1500 having  $\Phi_s^{(0)} = \Phi$  and for  $1 \leq t \leq T$ :

$$1501 \Phi_s^{(t)} = \Phi_s^{(t-1)} - \alpha \nabla_{\Phi_s^{(t-1)}} L(\Phi_s^{(t-1)} | \{s\}). \quad (25)$$

1502 Through the inner steps, we obtain the updated heatmap  $\theta_s^{(T)} = F_{\Phi_s^{(T)}}(D_s)$ . For each instance  $s$  in the  
1503 batch,  $K$  solutions  $\{\tau^1, \tau^2, \dots, \tau^K\}$  are sampled on the basis of  $\theta_s^{(T)}$  to calculate the reinforcement  
1504 learning-estimated gradient of  $\theta$ :

$$1505 \nabla_\theta \mathbb{E}_\tau [L(\tau)] = \mathbb{E}_\tau [(L(\tau) - S(s)) \nabla_\theta \log p_\theta(\tau)], \quad (26)$$

1506 where  $L(\cdot)$  denotes the length of a feasible tour and  $p_\theta$  is an auxiliary distribution to compute the  
1507 probability of a feasible solution for TSP with random start node and chain rule factorization:

$$1508 p_\theta(i_{n+1} | i_{n'} \leq n) = \frac{\exp(\mathbf{s}_{i_n, i_{n+1}})}{\sum_{n'=n+1}^N \exp(\mathbf{s}_{i_n, i_{n'}})}. \quad (27)$$

Subsequently, we optimize the performance of the graph neural network with the estimated gradient and a meta-objective, closing the outer loop:

$$L_{\text{meta}}(\Phi|C) = \mathbb{E}_{s \in C} S(\theta_s^{(T)}|s). \quad (28)$$

### E.1.3 RESULTS AND DISCUSSION

**Performance.** As demonstrated in Table 8, with our modified input node embeddings, DIMES works finely with our RedCO framework as a matrix encoder for general TSP, achieving comparable solving quality via active searching. Despite notable gap from DIMES to MatPOENet and MatD-IFNet, DIMES show good compatibility of RedCO and have the potential to effectively scale to larger instances, which can also be a valuable research direction in the future.

Table 8: Results of RedCO-DIMES trained on mixed problem data.

Scale	Methods	ATSP↓	2DTSP↓	DHCP (L↓, FR↑)		3SAT (L↓, FR↑)		Avg. L↓
20	DIMES	2.2335	4.1696	2.9448	2.67%	2.6660	2.12%	3.0035
	DIMES-AS(100)	1.6790	3.9092	0.4596	60.12%	0.2828	77.12%	1.5826
	DIMES-AS(200)	1.6439	3.8809	0.4464	61.92%	0.3068	75.16%	1.5695
50	DIMES	2.3341	6.6271	3.1788	1.56%	5.3656	0.12%	4.3764
	DIMES-AS(100)	1.6920	5.9447	0.5908	46.04%	1.5830	20.44%	2.4528
	DIMES-AS(200)	1.6794	5.9194	0.5000	54.20%	1.4296	23.36%	2.3821
100	DIMES	2.5186	9.5777	3.8064	1.16%	3.8064	0.00%	6.4018
	DIEMS-AS(100)	1.6968	8.3390	0.8480	24.00%	2.8040	7.16%	3.4220

**Efficiency.** Table 8 lists the solving efficiency of vanilla MatNet and DIMES under our RedCO framework. MatNet benefits from its light-weight architecture and sequential decision paradigm and have better time advantage. Active search process endows DIMES with better per-instance solving performance, while consumes much more time due to its gradient-based local search.

Table 9: Solving efficiency comparison under our RedCO framework. Setting:  $N \approx 50$ , batch\_size = 100, 2500 instances. DIMES( $T$ ): DIMES with  $T$  inner updates of active search.

Backbone	MatNet	MatNet(8×)	DIMES	DIMES(15)	DIMES(100)
Time	15s	2m40s	2m17s	10m35s	1h24m

**MatNet v.s. DIMES: MatNet wins on both efficiency and model performance, but DIMES has better scalability.** We compare vanilla MatNet without augmentation and DIMES without fine-tuning, both trained with mixed data. We see that MatNet outperforms DIMES significantly. We also present the solving time of vanilla MatNet and DIMES in Table 9, which demonstrates the high efficiency of MatNet. Though MatNet wins on both efficiency and model performance, according to their official papers, DIMES can be run on TSP-10,000 (Qiu et al., 2022), but MatNet only scales to about TSP-100 (Kwon et al., 2021), indicating better scalability of DIMES. It is because DIMES adopts a lighter neural architecture, but MatNet has a complex rollout scheme, causing a non-negligible amount of temporal variables, thus limiting its scalability.

**DIMES v.s. DIMES-AS( $T$ ): The trade-off between efficiency and effectiveness brought by fine-tuning on test cases.** By comparing DIMES-AS( $T$ ) with vanilla DIMES, DIMES-AS( $T$ ) improves DIMES significantly with fine-tuning on the test cases. However, DIMES-AS( $T$ ) may suffer from severe scalability issue in real-world applications. The solving time in Table 9 shows that DIMES(15) may take about 4.6 times as DIMES.

## E.2 MORE APPLICABLE PROBLEMS

### E.2.1 VERTEX COVER

**Definition 4** (Vertex Cover Problem (VC)). *Given an undirected graph  $G$  and a positive integer  $k$ , a vertex cover of  $G$  is a set  $S$  of vertices so that every edge is incident on at least one vertex of  $G$ . The problem is to determine whether  $G$  has a vertex cover of size no more than  $k$ .*

**Reduction from VC to HCP.** Let the (undirected) graph of VC instance be  $\mathcal{G}(\mathcal{V}, \mathcal{E})$  and the target is to determine whether there exists a vertex cover  $S$  containing no more than  $k$  vertices. We can construct an HCP graph  $\mathcal{G}'(\mathcal{V}', \mathcal{E}')$  with  $4|\mathcal{E}| + k$  vertices. Indexing the edges in  $\mathcal{E}$  from 1 to  $|\mathcal{E}|$ ,  $\mathcal{G}'$  can be mathematically described as:

$$\mathcal{V}' = \{a_1, a_2, \dots, a_k\} \cup \{[u, i, 0], [u, i, 1] | u \in \mathcal{V}, i \in \mathcal{E}\}, \quad (29)$$

where  $i$  is incident on  $u$ .

$$\begin{aligned} \mathcal{E}' = & \{([u, i, 0], [u, i, 1]) | [u, i, 0] \in \mathcal{V}'\} \\ & \cup \{([u, i, a], [v, i, a]) | i \in \mathcal{E}, i = (u, v), a \in \{0, 1\}\} \\ & \cup \{([u, i, 1], [u, j, 0]) | \nexists e \text{ s.t. } i < e < j, [u, e, 0] \in \mathcal{V}'\} \\ & \cup \{([u, i, 1], a_f) | 1 \leq f \leq k, \nexists e \text{ s.t. } e > i, [u, e, i] \in \mathcal{V}'\} \\ & \cup \{(a_f, [u, i, 0]) | 1 \leq f \leq k, \nexists e \text{ s.t. } e < i, [u, e, i] \in \mathcal{V}'\}. \end{aligned} \quad (30)$$

**Transform HCP Solution to VC Decision.** If there exists a Hamiltonian cycle  $\tau$  in  $\mathcal{G}'$ , we first select all vertices in  $\tau$  that connect any vertex in  $\{a_1, a_2, \dots, a_k\}$ . The selected vertices are necessarily in the form of  $\langle u, i, a \rangle$ , and all these  $u \in \mathcal{V}$  constitute the vertex cover of  $\mathcal{G}$  within  $k$  vertices.

Note that the VC problem has been incorporated in RedCO framework and implemented for evaluation. The details of data generation and empirical results are provided in Appendix F.4.

### E.2.2 CLIQUE PROBLEM

**Definition 5** (Clique Problem). *A clique is a (sub)graph induced by a vertex set  $K$  in which all vertices are pairwise adjacent, i.e., for all distinct  $u, v \in K$ ,  $(u, v) \in E$ . A clique of size  $k$  is denoted as  $K_k$ . The clique problem is to determine whether a graph on  $n$  vertices has a clique of size  $k$ .*

**Reduction from clique problem to SAT.** Given an clique instance, we introduce the following to for an SAT instance:

**Variables:**

$y_{i,r}$  (true if node  $i$  is the  $r$ -th node of the clique) for  $1 \leq i \leq n, 1 \leq r \leq k$ .

**Clauses:**

- 1) For each  $r$ ,  $y_{1,r} \vee y_{2,r} \vee \dots \vee y_{n,r}$  (some node is the  $r$ th node of the clique).
- 2) For each  $i, r < s$ ,  $\neg y_{i,r} \vee \neg y_{i,s}$  (no node is both the  $r$ -th and  $s$ -th node of the clique).
- 3) For each  $r \neq s$  and  $i < j$  such that  $(i, j)$  is not an edge of  $G$ ,  $\neg y_{i,r} \vee \neg y_{j,s}$ . (If there's no edge from  $i$  to  $j$  then nodes  $i$  and  $j$  cannot both be in the clique).

That's the entire formula that will be satisfiable if and only if  $G$  has a clique of size  $k$ . As SAT problem can be transformed to 3SAT and further reduced to general TSP in polynomial time, the decision of Clique problem can be solved by RedCO-empowered solvers.

### E.2.3 INDEPENDENT SET PROBLEM

**Definition 6** (Independent Set). *An independent set is vertex set  $S$  in which no two vertices are adjacent, i.e., for all distinct  $u, v \in S$ ,  $(u, v) \notin E$ .*

**Definition 7** (Complement Graph). *Let  $G = (V, E)$  be a graph, the complement graph of  $G$ , denoted as  $\bar{G} = (V, \bar{E})$ , is defined such that  $\bar{E}$  contains all the edges not present in  $G$ .*

Table 10: Ablation studies for the rough solver of MatNet-POE. Scale  $N \approx 50$ . Trained on mixed data, tested with 8x augmentation.

Methods	ATSP↓	2DTSP↓	DHCP (L↓, FR↑)		3SAT (L↓, FR↑)		Avg. L↓	Avg. FR↑
Non-MatNet-POE	1.7988	5.8178	0.4080	64.72%	1.0020	34.76%	2.2566	49.74%
FI-MatNet-POE	1.8370	6.0962	0.1920	82.80%	0.6060	55.72%	2.1828	69.26%
MatPOENet (NN)	<b>1.6417</b>	<b>5.7283</b>	<b>0.0172</b>	<b>98.28%</b>	<b>0.2456</b>	<b>77.60%</b>	<b>1.9082</b>	<b>87.94%</b>

By definition of complement,  $(u, v) \in E \leftrightarrow (u, v) \notin \bar{E}$ . The statement that  $S \subseteq V$  is an independent set in  $G$  is equivalent to the fact that  $S$  induces a clique in  $\bar{G}$ . Therefore, an IS problem can be transformed into a Clique decision, and solved by the same reduction of Clique problem to general TSP thereafter.

#### E.2.4 VEHICLE ROUTING PROBLEMS

While problems like CVRP cannot be directly solved by a direct transformation, the TSP solver can still be utilized. E.g, the Cluster-First Route-Second Method (Shalaby et al., 2021), solves CVRP by first clustering points and then solving each cluster as a TSP. Thus, a robust TSP solver is effective in the second phase for CVRP. Additionally, as mentioned in Ye et al. (2024b), large routing problems can be partitioned into TSPs and TSPs into Shortest Hamiltonian Path Problems (SHPPs), solidifying the significant role a good TSP solver plays targeting sub-structures of complex VRPs.

#### E.2.5 MATPOENET & MATDIFFNET AS PROBLEM-SPECIFIC SOLVER

In addition to the problems mentioned above that can be consistently learned and solved by reducing to general TSP, our proposed MatPOENet and MatDIFFNet can also serve as problem-specific individual solvers decoupled from RedCO, thus enabling a wider range of applicable problems, as long as specified in a matrix form of parameters quantifying the relationship between two groups of items. For instance, as evaluated in Kwon et al. (2021) and Li et al. (2023), Flexible Flow Shop Problem (FFSP) and Maximal Independent Set (MIS) problem are readily modelled for MatPOENet and MatDIFFNet, respectively.

**Conclusion.** Application of the reduction scheme to a wider range of problems are theoretically guaranteed by the computational complexity theory, and will be further studied in our future research. Note that resorting to problem reduction for general solving of different CO problems has limitations, where some tasks with more complicated constraints or high transformation complexity are not practical. However, the orthogonality between RedCO and specific solvers should be noted, as more problems has the potential to be solved via individual modelling for our proposed neural solvers.

## F SUPPLEMENTARY EXPERIMENTS

### F.1 FURTHER EXPERIMENTS OF POE

**Different Initial Rough Solvers.** As mentioned in RQ4 in the main context, we tested different solvers to prepare the rough solution to initialize POE. In Table 10, among nearest neighbor (NN), farthest insertion (FI) and without initial solution (Non), NN outperforms the others, which proves the efficacy of choosing the simple nearest neighbor heuristic as initial rough solver to capture local information for POE.

**Different Initial Node Embeddings.** As mentioned in RQ4 in the main context, we have additionally implemented the two advisable ways mentioned as alternative initial embeddings for MatNet in its paper (Kwon et al., 2021). Note that they are both aimed at breaking the dimension restriction as our proposed POE.

Through this experiment and results in Table 11, we acknowledge the potential capability of tailored trainable embeddings and anticipate further studies, though, within our time and knowledge, better performance is achieved using our proposed POE over vanilla random vectors or trainable parameter matrices of the same shape.

Table 11: Results of MatNet model equipped with different initial node embeddings on  $N \approx 50$  dataset. “Trainable”:  $N_{\max}$  different vectors made of learnable parameters. “Random”: completely random vectors for each problem instance.

Init. Embed. Type	ATSP↓	2DTSP↓	DHCP (L↓, FR↑)		3SAT (L↓, FR↑)		Avg. L↓
MatNet-Random	2.1044	5.8981	0.8560	33.20%	1.1620	30.44%	2.5051
MatNet-Trainable	1.8923	5.8157	0.4148	63.96%	0.5012	58.52%	2.1560
MatPOENet (ours)	<b>1.6417</b>	<b>5.7283</b>	<b>0.0172</b>	<b>98.28%</b>	<b>0.2456</b>	<b>77.60%</b>	<b>1.9082</b>

## F.2 PRETRAINING-FINETUNING APPLICATIONS

As claimed in the main context that our proposed RedCO serves properly as a pretraining-finetuning framework, we hereby present two supportive experiments in conventional scenarios:

**i) Cross-task scenario:** pretrained on several problem types, finetuned on an unseen problem type.

Table 12: Results of the cross-task finetuning on 3SAT. MatPOENet is pretrained under RedCO framework with dataset comprising ATSP, 2DTSP and DHCP instances of  $N \approx 50$  for 2,000 epochs and subsequently finetuned on the new task of 3SAT data for (a much fewer) 500 iterations.

Description	3SAT (L)↓	3SAT(FR)↑	#Epochs
Pretrained on ATSP, 2DTSP, DHCP w/o Finetuning	1.4080	17.92%	2000
Pretrained on ATSP, 2DTSP, DHCP w/ Finetuning on 3SAT	0.0404	95.96%	50
	0.0360	96.40%	100
	0.0292	97.08%	200
Trained on merely 3SAT (control group)	0.0400	96.08%	2000

From Table 12, We observe that after finetuning on the unseen task data (3SAT), the model performance is improved significantly compared with that without finetuning (the first row of the table), and can yield a similar performance compared to the case where the model is primarily trained on 3SAT only (the third row of the table). These results demonstrate the applicability of RedCO for pretraining-finetuning, which also directs a feasible path to address the generalizability issue of MatNet-POE.

**ii) Cross-scale scenario:** pretrained on smaller scaled dataset, finetuned on larger scaled dataset.

Table 13: Results of the cross-scale finetuning experiments on  $N \approx 100$  sets. The MatPOENet model is pretrained under RedCO framework with different dataset of  $N \approx 50$  for 2,000 epochs and subsequently finetuned on mixed data of  $N \approx 100$  scale for (a much fewer) 500 iterations.

Pretrain data	Finetune data	ATSP↓	2DTSP↓	DHCP (L↓, FR↑)		3SAT (L↓, FR↑)		Avg. L↓
Mixed-50	-	2.5656	8.5404	23.5064	0.00%	17.5564	0.00%	13.0422
Mixed-50	Mixed-100	1.9798	<b>8.0573</b>	1.7796	6.60%	2.0664	11.68%	3.4708
ATSP-50	Mixed-100	<b>1.8855</b>	8.3838	<b>0.6712</b>	<b>46.72%</b>	0.2888	72.76%	<b>2.8073</b>
Mixed-100	-	1.8655	8.1719	0.0052	99.48%	<b>0.2440</b>	<b>77.12%</b>	2.5717

Remarkably, we observed from Table 13 that pretraining on smaller instances of ATSP leads to greatly improved outcomes when fine-tuned on larger scaled multi-task datasets, possibly suggesting the significance of capturing general problem patterns as well as handling hard cases during pretraining. The bold numbers are the best among finetuned settings, approaching competitive performance of the model primarily trained on  $N \approx 100$  data (the last row) with much shorter training time.

These empirical findings provide strong support for our assertion regarding RedCO’s capability to serve as a pretraining-finetuning framework. Furthermore, they spark further interest and exploration into leveraging this paradigm to enhance the model’s scalability as well as generalization performance.



F.3 COMPARISON OF LEARNING PARADIGMS

We have already tried to combine the idea of instance reduction to general TSP with **supervised** approach. To ensure fair competition, we modified MatNet architecture into a heavy-encoder and light-decoder model for SL, which by convention, outputs a heatmap to guide subsequent local searches. Note that calculating supervision solutions for ATSP/2DTSP at scale is extremely time-consuming, we implemented the method on decision problem (HCP and 3SAT) instances where the ground truth is easier to obtain.

Table 14: Performance comparison for HCP and 3SAT problems with different learning paradigms under RedCO.

Method	HCP-50 (L↓)	FR↑	Time	3SAT-50 (L↓)	FR↑	Time
Greedy	6.014	0.04%	0s	5.987	0.00%	0s
LKH	0.000	100.00%	1m29s	0.140	86.28%	2m11s
MatNet	0.481	53.04%	4m12s	0.329	73.12%	2m
RedCO-RL	0.017	98.28%	4m8s	0.117	88.44%	2m4s
RedCO-SL	<b>0.000</b>	<b>100.00%</b>	<b>2m29s</b>	<b>0.077</b>	<b>92.32%</b>	<b>2m39s</b>

Table 15: Performance comparison for larger HCP and 3SAT problems with different learning paradigms under RedCO.

Method	HCP-500 (L↓)	FR↑	Time	3SAT-500 (L↓)	FR↑	Time
Greedy	6.924	0.00%	1m27s	15.149	0.00%	1m15s
LKH	0.526	55.88%	1h1m	5.812	3.92%	1h10m
RedCO-SL	<b>0.127</b>	<b>88.12%</b>	<b>1h24m</b>	<b>2.124</b>	<b>65.60%</b>	<b>1h22m</b>

Results show that SL paradigm also works performantly under our RedCO framework, with better scalability but more preliminary overheads for supervision and post searching. (RedCO-RL refers to MatPOENet)

F.4 RESULTS ON VERTEX COVER PROBLEM

Echoing the introduction of more applicable problems in Appendix E.2, we have conducted additional experiments on vertex cover (with 2500 test cases on  $N \approx 50$ ), following the reduction procedures provided. Similar to the SAT-distributed general TSP, we specified the important parameters for data generation as specified in Table 16. The experimental results are shown in Table 17.

Table 16: Parameters for vertex cover instance generation.

TSP Scale $N$	Num_Edges $E$	Cover Size $k$	Num_Nodes $N_{VC}$	Range of $N$	Average $N$
$N \approx 50$	<i>Uniform</i> (10, 12)	<i>Uniform</i> (3, 8)	<i>Uniform</i> (8, 17)	[43, 56]	50.0

Note that our initial experimental results show that our proposed models are easily adaptable into the RedCO framework and perform decently on the new problem VC. With the transformation of complementary graphs, a series of node selection tasks on the graph could also be addressed similarly. Thus far, a representative range of edge-wise tasks (TSP, ATSP, HCP), node-wise tasks (VC, Clique,

Table 17: Results on vertex cover.

Method	Tour length (↓)	Found rate (↑)
GUROBI	0.000	100.00%
Greedy	7.351	0.00%
MatNet	2.349	1.08%
MatPOENet-8x	0.220	78.28%
MatDIFFNet-2OPT	0.477	66.60%

Table 18: Performance comparison on standard symmetric TSP-50 test set.

Method	Tour length ( $\downarrow$ )	Optimality gap ( $\downarrow$ )	Time/instance
Concorde (Optimal)	5.688	–	0.074s
AM (Kool et al., 2018)	5.747	1.04%	< 0.001s
POMO (Kwon et al., 2020)	5.698	0.18%	< 0.001s
Sym-NCO (Kim et al., 2022)	5.738	0.68%	< 0.001s
GCN (Joshi et al., 2019)	5.776	1.53%	0.008s
UTSP+MCTS (Min et al., 2024)	5.818	2.30%	0.063s
DIMES+S+AS (Qiu et al., 2022)	5.859	3.01%	2.884s
DIFUSCO (Sun & Yang, 2023)	5.709	0.38%	0.388s
T2T+GS (Li et al., 2023)	5.690	0.04%	1.164s
GNNGLS-1s (Hudson et al., 2021)	5.693	0.10%	1.080s
MatNet-8x (Kwon et al., 2021)	5.857	2.97%	0.056s
MatPOENet*-8x (Ours)	5.781	1.63%	0.059s
MatPOENet*-128x (Ours)	5.726	0.66%	0.296s
MatDIFFNet-2OPT (Ours)	5.721	0.59%	0.509s

Table 19: Performance comparison on standard symmetric TSP-100 test set.

Method	Tour length ( $\downarrow$ )	Optimality gap ( $\downarrow$ )	Time/instance
Concorde (Optimal)	7.756	–	0.404s
AM (Kool et al., 2018)	7.951	2.52%	< 0.001s
POMO (Kwon et al., 2020)	7.883	1.64%	0.001s
Sym-NCO (Kim et al., 2022)	7.927	2.21%	< 0.001s
GCN (Joshi et al., 2019)	8.307	7.08%	0.011s
UTSP+MCTS (Min et al., 2024)	8.069	4.46%	0.223s
DIMES+S+AS (Qiu et al., 2022)	8.061	3.94%	8.508s
DIFUSCO (Sun & Yang, 2023)	7.845	1.14%	0.409s
T2T+GS (Li et al., 2023)	7.788	0.13%	1.198s
GNNGLS-1s (Hudson et al., 2021)	7.837	1.05%	1.389s
MatPOENet*-8x (Ours)	8.127	4.78%	0.262s
MatPOENet*-128x (Ours)	7.933	2.28%	0.758s
MatDIFFNet-2OPT (Ours)	7.840	1.08%	0.769s

etc.) and decisive problem (SAT) combined have formed a good coverage of mainstream COPs on graphs. In the future, we will delve further into the detailed implementation and improvements on the instance-level performance and work on more problems.

## F.5 RESULTS ON STANDARD SYMMETRIC TSP

To better align our work with previous literature in pursuit of 2D TSP, additional experiments have been conducted on the consistent test dataset of symmetric TSP-50 and TSP-100. Each dataset consists of 1280 instances featured by node coordinates. Results are shown in Table 18 and Table 19. The results of previous works are re-implemented or re-executed with the provided model weights within our consistent evaluation environment to ensure fair comparison.

**Note.** All methods except MatNet and those proposed in this paper adopt 2D coordinates as input node features. In contrast, our methods solely encode the distance matrix as input information. Additionally, our models can be trained on mixed data, whereas previous works were exclusively trained on symmetric TSP only. These comparative results demonstrate that our models can achieve comparable (and even better in some cases) performance without utilizing coordinates, validating our proposed MatPOENet and MatDIFFNet as successful matrix encoders for symmetric TSP.

## F.6 RESULTS ON REAL-WORLD INSTANCES

Table 20: Tested 45 TSPLIB instances of scale range: [14, 195]

att48.tsp	berlin52.tsp	ch130.tsp	ch150.tsp	eil101.tsp
eil51.tsp	eil76.tsp	kroA100.tsp	kroC100.tsp	kroD100.tsp
lin105.tsp	pr76.tsp	rd100.tsp	st70.tsp	bayg29.tsp
bays29.tsp	brg180.tsp	fri26.tsp	gr120.tsp	gr24.tsp
gr48.tsp	gr96.tsp	ulysses16.tsp	ulysses22.tsp	bier127.tsp
d198.tsp	kroA150.tsp	kroB100.tsp	kroB150.tsp	kroE100.tsp
pr107.tsp	pr124.tsp	pr136.tsp	pr144.tsp	pr152.tsp
rat195.tsp	rat99.tsp	u159.tsp	brazil58.tsp	dantzig42.tsp
gr17.tsp	gr21.tsp	hk48.tsp	swiss42.tsp	burma14.tsp

Table 21: Results on TSPLIB instances.

Method	Avg. tour length
LKH3	4.8622
Greedy	5.4455
MatPOENet	5.0811
MatDIFFNet	5.2744

In the main experiment, this paper primarily focuses on synthetic data for testing. To address this limitation, we have additionally tested our methods on a subset of standard TSPLIB instances, which are renowned for their real-world scenarios in TSP evaluation. We selected 45 instances with city scales ranging from 14 to 195 (as listed in Table 20). These instances encompass different distance types (such as “EUC\_2D”, “GEO”, etc.) and representation formats (such as “coordinates”, “full matrix”, “diagonal matrix”, etc.). To ensure a fair evaluation and optimally leverage the matrix-encoding capability of our unified framework and models, we have rewritten the selected instances into a consistent format of ‘EDGE\_WEIGHT\_TYPE: EXPLICIT’ and ‘EDGE\_WEIGHT\_FORMAT: FULL\_MATRIX’, with all distances scaled to  $[0, 1]$ . The results are given in Table 21.

The results demonstrate that our models are also effective on problem instances with completely unseen distributions and varying sizes. We would like to kindly remind the readers that an important aspect is that we are the first to evaluate the TSPLIB instances without any initial knowledge from node coordinates. Thank you again for enhancing the completeness of our evaluation. The task of improving the generalizability towards more real-world cases are planned for future research.

## F.7 FULL EXPERIMENTAL RESULTS

For your quick reference, we present a complete version of experimental results in Table 22, supplementary to Table 2 in the main context, containing both major results and most additional results. A substantial quantity of empirical investigations are conducted to provide a comprehensive evaluation of our proposed framework and models.

## G FURTHER DISCUSSIONS

### G.1 NOTE ON LKH

We have been conducting a preliminary study on the boundary of the strong heuristic LKH when dealing with general TSP beyond the 2D Euclidean space where it holds an overwhelming advantage. LKH is a heuristic with three main components: the  $\alpha$ -nearest measure, node penalties, and the  $k$ -opt searching algorithm. It operates in the following steps:

1. Compute the  $\alpha$ -Nearest Measure: The  $\alpha$ -measure of an edge is calculated based on the length of the minimum 1-tree of a graph and the minimum 1-tree containing that edge. The  $\alpha$ -measures are used to specify the edge candidate set.
2. Node Penalties: LKH employs a subgradient optimization technique to obtain penalties over each node and modifies the distances.

Table 22: Full experimental results. Reported data for ATSP and 2DTSP are four length. “Single”: models trained and tested on each problem respectively. “Mixed”: unified models trained with a mixture of 4 tasks on each scale. Asterisk (\*): a unified model trained with a mixture of 4 tasks and 3 scales. ‘8x’: representing 8 parallel trials for sequential model solving. BQ-NCO (Drakulic et al., 2023) and GOAL (Drakulic et al., 2024) reports their results on ATSP but have not been open-sourced yet. We make estimation according to their reported optimality gap for reference only. **Bold**: the best score of neural solvers in each column. Underlined: the best solved length over the full set for reference. **Red box** and **blue box**: ours that outperform LKH with max\_trials=10,000 and max\_trials=500 respectively. **Time**: the average time (seconds) per instance solving over each line, with batch size set to 1.

ID	Methods	Train Data	ATSP↓	2DTSP↓	DHCP (L↓, FR↑)	3SAT (L↓, FR↑)	Avg. L↓	Avg. Gap↓	Avg. FR↑	Time		
1	Gurobi	-	1.5349	3.8347	0.0000	100.00%	0.0000	100.00%	1.3424	100.00%	0.135	
2	LKH (10000)	-	1.5349	3.8347	0.0008	99.92%	0.0000	100.00%	1.3426	0.01%	99.96%	0.327
3	LKH (500)	-	1.5349	3.8347	0.0056	99.44%	0.0000	100.00%	1.3438	0.11%	99.72%	0.038
4	Nearest Neighbor	-	2.0069	4.5021	3.8556	0.48%	3.0504	0.32%	3.3428	149.02%	0.40%	0.000
5	Farthest Insertion	-	1.7070	3.9695	3.3136	1.76%	4.8816	0.00%	3.4679	158.34%	0.88%	0.000
6	MatNet	ATSP	1.5871	4.2612	2.9608	1.12%	3.4772	0.56%	3.0716	128.82%	0.84%	0.005
7	MatNet-8x	ATSP	<b>1.5391</b>	3.9735	1.5476	9.28%	1.9184	6.08%	2.2446	67.21%	7.68%	0.036
8	MatNet	Mixed	1.6359	3.9114	0.9740	27.60%	3.4656	11.04%	2.4967	85.99%	19.32%	0.005
9	MatNet-8x	Mixed	1.5645	3.8478	0.1936	80.92%	1.6272	1.36%	1.8083	34.71%	41.14%	0.037
10	Non-MatNet-POE	Mixed	1.7133	3.8990	0.8400	33.24%	0.5760	50.64%	1.7571	30.89%	41.94%	0.005
11	Non-MatNet-POE-8x	Mixed	1.6057	3.8695	0.5444	53.28%	0.3344	67.52%	1.6057	19.62%	60.40%	0.035
12	DIMES	Mixed	2.2335	4.1696	2.9448	2.67%	2.6660	2.12%	3.0035	123.74%	2.39%	0.035
13	DIMES-AS(100)	Mixed	1.6790	3.9092	0.4596	60.12%	0.2828	77.12%	1.5826	17.90%	68.62%	0.522
14	DIMES-AS(200)	Mixed	1.6439	3.8809	0.4464	61.92%	0.3068	75.16%	1.5695	16.92%	68.54%	1.124
15	MatPOENet	Mixed	1.6445	3.8643	0.8676	32.60%	0.4540	61.88%	1.7076	27.21%	47.24%	0.006
16	MatPOENet-8x	Mixed	1.5695	3.8389	0.1760	82.68%	0.0112	98.88%	1.3989	4.21%	90.78%	0.043
17	MatPOENet*	Mixed	1.5933	3.8632	0.4052	62.24%	0.1528	84.88%	1.5036	12.01%	73.56%	0.006
18	MatPOENet* 8x	Mixed	<b>1.5006</b>	<b>3.8372</b>	<b>0.0556</b>	<b>94.44%</b>	<b>0.0008</b>	<b>99.92%</b>	<b>1.3610</b>	<b>1.39%</b>	<b>97.18%</b>	<b>0.043</b>
19	Gurobi	-	1.5545	5.6952	0.0000	100.00%	0.0000	100.00%	1.8124	-	100.00%	0.296
20	LKH (10000)	-	1.5548	5.6953	0.0000	100.00%	0.2784	74.80%	1.8821	3.85%	87.40%	0.513
21	LKH (500)	-	1.5557	5.6964	0.0000	100.00%	0.4796	61.80%	1.9329	6.65%	80.90%	0.059
22	Nearest Neighbor	-	2.0945	6.9977	5.1120	0.00%	5.9872	0.00%	5.0548	178.90%	0.00%	0.000
23	Farthest Insertion	-	1.8387	6.0998	4.0224	5.28%	10.3964	0.00%	5.5893	208.39%	2.64%	0.001
24	MatNet	ATSP	1.5753	7.3618	1.4856	11.80%	8.4020	0.00%	4.7062	159.67%	5.90%	0.007
25	MatNet-8x	ATSP	<b>1.5612</b>	6.9445	0.6036	49.24%	6.3468	0.00%	3.8640	113.20%	24.62%	0.061
26	MatNet	Mixed	1.8098	6.0000	0.9288	30.84%	1.1900	30.52%	2.4821	36.95%	30.68%	0.007
27	MatNet	Mixed	1.7340	5.8664	0.3056	71.52%	0.2992	73.08%	2.0513	13.18%	72.30%	0.007
28	Non-MatNet-POE	Mixed	1.8606	5.8855	1.0392	27.28%	1.1416	31.32%	2.4817	36.93%	29.30%	0.007
29	Non-MatNet-POE-8x	Mixed	1.7988	5.8178	0.4080	64.72%	1.0020	34.76%	2.2566	24.51%	49.74%	0.060
30	Rand-MatNet-POE	Mixed	1.8282	6.0207	0.9380	30.00%	1.4404	22.12%	2.5568	41.07%	26.06%	0.006
31	Rand-MatNet-POE-8x	Mixed	1.7513	5.8853	0.3096	71.52%	0.4708	60.84%	2.1042	16.10%	66.18%	0.063
32	FI-MatNet-POE-8x	Mixed	1.8370	6.0962	0.1920	82.80%	0.6060	55.72%	2.1828	20.44%	69.26%	0.064
33	MatNet-Random-8x	Mixed	2.1044	5.8981	0.8560	33.20%	1.1620	30.44%	2.5051	38.22%	31.82%	0.064
34	MatNet-Trainable-8x	Mixed	1.8923	5.8157	0.4148	63.96%	0.5012	58.52%	2.1560	18.96%	61.24%	0.071
35	GLOP	Single	1.8885	6.6499	3.7244	0.84%	4.9816	0.76%	4.3111	137.87%	0.80%	0.115
36	DIMES	Mixed	2.3341	6.6271	3.1788	1.56%	5.3656	0.12%	4.3764	141.47%	0.84%	0.055
37	DIMES-AS(100)	Mixed	1.6920	5.9447	0.5908	46.04%	1.5830	20.44%	2.4528	35.33%	33.24%	2.016
38	DIMES-AS(200)	Mixed	1.6794	5.9194	0.5000	54.20%	1.4296	23.36%	2.3821	31.43%	38.78%	3.879
39	MatPOENet-8x	Single	<b>1.5643</b>	<b>5.7042</b>	0.0652	93.52%	0.1888	81.72%	<b>1.8806</b>	<b>3.76%</b>	87.62%	0.066
40	MatPOENet	Mixed	1.6881	5.7694	0.1444	86.20%	1.3644	27.08%	2.2416	23.68%	56.64%	0.009
41	MatPOENet-8x	Mixed	1.6417	<b>5.7283</b>	<b>0.0172</b>	<b>98.28%</b>	0.2456	77.60%	1.9082	5.29%	87.94%	0.067
42	MatPOENet*	Mixed	1.6753	5.8633	0.2112	80.48%	0.8172	42.40%	2.1417	18.17%	61.44%	0.008
43	MatPOENet* 8x	Mixed	1.6285	5.7575	0.0280	<b>97.20%</b>	<b>0.1172</b>	<b>88.44%</b>	1.8828	3.88%	<b>92.82%</b>	0.067
44	MatPOENet-8x ( $N > d$ )	Mixed	1.8799	5.9742	0.4548	60.24%	0.3292	75.56%	2.1595	19.15%	68.00%	0.062
45	MatDIFFNet	Single	2.0713	5.7954	2.0992	15.32%	<b>0.0464</b>	<b>98.16%</b>	2.5031	38.11%	56.74%	0.157
46	MatDIFFNet-2OPT	Single	1.7186	5.7279	0.8324	44.08%	<b>0.0188</b>	<b>98.64%</b>	2.0744	14.46%	71.36%	0.165
47	MatDIFFNet	Mixed	1.8385	6.2332	2.0648	15.76%	0.1112	94.68%	2.5619	41.35%	55.22%	0.155
48	MatDIFFNet-2OPT	Mixed	1.6591	5.8619	0.8192	44.52%	0.0496	95.64%	2.0975	15.73%	70.08%	0.164
49	Gurobi	-	1.5661	7.7619	0.0000	100.00%	0.0000	100.00%	2.3320	-	100.00%	0.689
50	LKH (10000)	-	1.5674	7.7709	0.0000	100.00%	1.0008	44.80%	2.5848	10.84%	72.40%	0.811
51	LKH (500)	-	1.5704	7.8015	0.0000	100.00%	1.6656	28.08%	2.7594	18.33%	64.04%	0.095
52	Nearest Neighbor	-	2.1321	9.6696	5.4016	0.20%	8.3236	0.00%	6.3859	173.84%	0.10%	0.002
53	Farthest Insertion	-	1.9333	8.4847	3.1256	26.64%	23.5160	0.00%	9.2649	297.29%	13.32%	0.003
54	MatNet	ATSP	<b>1.6217</b>	19.0644	17.8620	0.00%	40.1188	0.00%	19.6667	743.34%	0.00%	0.015
55	MatNet-8x	ATSP	1.5983	17.8146	13.5196	0.00%	35.3216	0.00%	17.0635	631.71%	0.00%	0.094
56	MatNet	Mixed	1.9849	8.2551	0.9776	31.68%	2.0408	13.84%	3.3146	42.14%	22.76%	0.018
57	MatNet-8x	Mixed	1.9210	8.1028	0.3640	69.60%	0.7740	50.76%	2.7904	19.66%	60.18%	0.095
58	GLOP	Single	1.8491	8.8849	2.7850	2.00%	6.4280	0.08%	4.9868	113.84%	1.04%	0.176
59	BQ-NCO	ATSP	1.5904	-	-	-	-	-	-	-	-	0.016
60	GOAL	ATSP	<b>1.5771</b>	-	-	-	-	-	-	-	-	0.039
61	Non-MatNet-POE	Mixed	2.0307	8.9929	1.0616	28.76%	1.2944	26.88%	3.3449	43.43%	27.82%	0.015
62	Non-MatNet-POE-8x	Mixed	1.9800	8.7895	0.4420	63.60%	1.0796	31.80%	3.0728	31.77%	47.70%	0.093
63	DIMES	Mixed	2.5186	9.5777	3.8064	1.16%	3.8064	0.00%	6.4018	174.52%	0.58%	0.124
64	DIMES-AS(100)	Mixed	1.6968	8.3390	0.8480	24.00%	2.8040	7.16%	3.4220	46.74%	15.58%	8.437
65	MatPOENet	Mixed	1.9183	8.2987	0.0984	90.28%	1.0704	32.32%	2.8465	22.06%	61.30%	0.017
66	MatPOENet-8x	Mixed	1.8655	8.1719	0.0052	99.48%	<b>0.2440</b>	<b>77.12%</b>	2.5717	10.28%	<b>88.30%</b>	0.094
67	MatPOENet*	Mixed	1.8107	8.2703	0.0796	92.12%	1.2856	26.04%	2.8616	22.71%	59.08%	0.017
68	MatPOENet* 8x	Mixed	1.7607	<b>8.0817</b>	<b>0.0012</b>	<b>99.88%</b>	0.3244	70.92%	<b>2.5420</b>	<b>9.01%</b>	85.40%	0.095
69	MatDIFFNet	Single	1.9432	7.9684	4.4536	2.96%	0.0404	98.44%	3.6014	54.43%	50.70%	0.103
70	MatDIFFNet-2OPT	Single	1.7165	<b>7.8482</b>	1.1404	37.72%	<b>0.0240</b>	<b>98.60%</b>	2.6823	15.02%	68.16%	0.112
71	MatDIFFNet	Mixed	1.8763	8.9030	3.2524	5.68%	0.1940	90.52%	3.5564	52.50%	48.10%	0.102
72	MatDIFFNet-2OPT	Mixed	1.6965	8.1804	0.9148	43.04%	0.0952	91.44%	2.7217	16.71%	67.24%	0.114

- 1944 3. Search Solutions by  $k$ -Opt:  $k$  edges in the current tour are exchanged by another set of  $k$   
 1945 edges from the candidate sets to improve the tour until no more exchanges can be found.  
 1946

1947 There is a fatal flaw of LKH on binary TSP (such as the SAT-distributed TSP in our case) in the first  
 1948 step of computing  $\alpha(i, j)$ . For a discrete TSP problem instance,  $\alpha(i, j)$  can only be either 0 or 1.  
 1949 This implies that many edges may have the same  $\alpha(i, j)$  value of 0, making it difficult to distinguish  
 1950 effective candidates and consequently leading to suboptimal performance on such discrete instances.  
 1951 Moreover, unlike the generation of HCP instances in our experiments where the ones and zeros are  
 1952 randomly sampled from a uniform distribution and a zero-length cycle is forced in each problem  
 1953 matrix, the 3SAT-distributed TSP cases are more complex due to their highly structured translation  
 1954 from variables and clauses to the HCP distance matrix. One possible approach to address this problem  
 1955 is to use a learned neural mapping network to transform some difficult binary distance matrices into  
 1956 the more softened and thus easier space to assist LKH solving.

## 1957 G.2 NOTE ON THE SCALABILITY AND APPLICABILITY

1958 Scalability remains one of the most frequently encountered challenges in the field of neural combina-  
 1959 torial optimization. The following is a conclusion of our observations and clarifications regarding the  
 1960 scalability issue, based on our investigations and experiments.  
 1961

1962 **Current Status of General TSP Solving.** Firstly, as demonstrated by the main experiments (Ta-  
 1963 ble 22), although the scale of the tested instances is not extremely large, the baseline TSP solvers  
 1964 (including both neural methods and strong heuristics such as LKH3) do not yield satisfactory results  
 1965 within an acceptable time frame. This indicates that for the relatively underexplored task of general  
 1966 TSP, the solvers at the current scale are still insufficiently effective, not to mention generalizing to  
 1967 larger scales.  
 1968

1969 **A Shared Convention.** From a peer perspective, a common phenomenon can be observed in top  
 1970 published literature targeting “multi-task”, “general”, and even “universal” combinatorial optimiza-  
 1971 tion, that an evaluation on problems with up to 100 nodes is generally an acknowledged convention.  
 1972 Table 6 presents a recent review of these works, ranging from the applicable problems to the evaluated  
 1973 scales of tasks.

1974 **Technical Limitations.** The training of MatPOENet consumes  $O(N^3)$  space ( $O(N^2)$  space for  
 1975 the attention mechanism and  $O(N)$  space for  $N$  rollout iterations), making it impractical to run on  
 1976 large-scale instances (e.g.,  $N \geq 500$ ) on a single GPU. However, as shown in Table 5, RedCO’s  
 1977 ability to learn larger-scaled instances can be achieved by switching to different learning paradigms.  
 1978 For example, a modified version of heatmap-based MatPOENet performs well on  $N \approx 500$  through  
 1979 vanilla supervised learning. Another approach to improving the ability to solve large-scale combina-  
 1980 torial optimization problems is to resort to the divide-and-conquer paradigm, which is also a consensus  
 1981 and has been proven feasible and effective (Ye et al., 2024b; Fu et al., 2021; Luo et al., 2024). In this  
 1982 context, a strong solver for small-to-medium-sized instances remains of irreplaceable importance. We  
 1983 have readily incorporated the latest work GLOP, which significantly enhances MatNet’s scalability.  
 1984 Moreover, the promising generative models for discrete optimization can be considered as detailed in  
 1985 Appendix G.4, which is also planned for our future work.

## 1986 G.3 DISCUSSION OF MATPOENET V.S. MATDIFFNET

1987 **A Trade-off among Quality, Efficiency, and Scalability.** As shown in the main result table,  
 1988 MatPOENet excels at smaller instances as a strong yet compact solver with faster inference and more  
 1989 transparent training process but can hardly scale due to its RL nature, whereas MatDIFFNet has more  
 1990 potential to scale to larger cases with more accurate proximity of the solution space (especially in  
 1991 continuous 2DTSP and complex discrete space, e.g., 3SAT) via its generative design but consumes  
 1992 much longer time to train and infer due to its heavier architecture and diffusion processes.  
 1993

1994 **Comparison of Stability.** MatDIFFNet does not directly generate solutions but decodes the heatmap  
 1995 to obtain them. Consequently, the solution quality of MatDIFFNet is less stable than that of Mat-  
 1996 POENet. Specifically, in the case of MatDIFFNet, if there is an error in predicting a particular node,  
 1997 it will directly impact the predictions of all subsequent nodes. In contrast, MatPOENet generates  
 solutions step by step and can select better subsequent nodes based on the current state even if there

1998 is an error in a particular node. This instability also results in the relatively poor performance of  
1999 MatDIFFNet when solving the Hamiltonian cycle problem (HCP).  
2000

#### 2001 G.4 DISCUSSION OF GENERATIVE COMBINATORIAL OPTIMIZATION 2002

2003 **Strong scalability of neural backbone and sparsification.** In addition to the fact that SL-based  
2004 neural networks generally outperform their RL counterparts in terms of scalability, MatDIFFNet  
2005 employs a GNN as the backbone encoder, which enables convenient graph sparsification (e.g., k-  
2006 nearest neighbor) on TSP. This effectively reduces computational overhead and improves inference  
2007 efficiency. As demonstrated in previous research (Qiu et al., 2022), training TSP solvers with a  
2008 sparsification factor of, for example 50, significantly reduces the memory and time overhead when  
2009 training graphs with while maintaining competitive performance. This is also one of the crucial  
2010 reasons we choose general TSP, an edge-based selection task, as the endpoint for problem reduction.  
2011 In contrast, such an edge sparsification scheme cannot be adopted when learning to solve most  
2012 node-based selection problems, such as vertex cover and independent set.

2013 **Rich expressivity of learning solution space distribution.** In our investigation of recent literature  
2014 on neural solving of combinatorial optimization, especially for graph problems like TSP, a notable  
2015 observation is the growing attention and demonstrated performance of diffusion-based generative  
2016 models (Sun & Yang, 2023; Li et al., 2023). From DIFUSCO and T2T to our proposed MatDIFFNet  
2017 and its future versions, generative models possess powerful expressive and modeling capabilities.  
2018 They can learn the distribution of high-quality solutions conditioned on specific problem instances,  
2019 which is beneficial for providing a good starting point or exploration direction in the solution space.  
2020 In the context of combinatorial optimization, this means they can potentially generate a variety of  
2021 solutions that might be closer to the optimal one, rather than being limited to a single or a few  
2022 predicted solutions as in some traditional methods.

2023 **Good prospects of consistency model and unsupervised tuning.** Moreover, the latest research on  
2024 generative combinatorial optimization indicates that diffusion models can be improved through con-  
2025 sistency training (Song & Dhariwal). Consistency models learn to map directly from different noise  
2026 levels to the optimal solution for a given instance, thereby achieving a high-quality, rapid one-step gen-  
2027 eration solution. This approach reduces the number of iterations and enhances efficiency. Therefore,  
2028 we will introduce consistency models into our framework in the future to optimize the inference speed  
2029 and computational efficiency of diffusion models. Also, as suggested in works (Sanokowski et al.,  
2030 2023; 2024), diffusion models finely foster the applicability of unsupervised learning of combinatorial  
2031 optimization.

2032 For these reasons, it is appropriate to present MatDIFFNet in parallel with MatPOENet in the main  
2033 context. This represents both conventional powerful autoregressive solvers using reinforcement  
2034 learning and a model with wider extendability and value for further exploration. We maintain that  
2035 this provides a more comprehensive view of the current trend in neural combinatorial optimization.  
2036  
2037  
2038  
2039  
2040  
2041  
2042  
2043  
2044  
2045  
2046  
2047  
2048  
2049  
2050  
2051